Creep of Cracked Fiber Reinforced Concrete

by

Megha Rajendrakumar Gohel

A Thesis Presented in Partial Fulfillment
of the Requirements for the Degree
Master of Science

Approved April 2017 by the
Graduate Supervisory Committee:

Barzin Mobasher, Chair
Subramaniam Dharmarajan
Narayanan Neithalath

ARIZONA STATE UNIVERSITY
May 2017

ABSTRACT

The concept of Creep is a term used to define the tendency of stressed materials to develop an increasing strain through time under a sustained load, thus having an increase in deflection or having an elongation with time in relation to the short term strain. While the subject of compression creep of concrete is well developed, use of concrete under tension loads has been limited at best due to brittleness of concrete. However with the advent of using fiber reinforced concrete, more and more applications where concrete is expected to carry tensile loads due to incorporation of fibers is gaining popularity. While the creep behavior of concrete in tension is important, the main case of the study is what happened when the concrete that is cracked in service is subjected to sustained loads causing creep. The relationship of opening cracks under these conditions are of utmost importance especially when the serviceability criteria is addressed. Little work has been reported in literature on the long-term behavior of FRC under sustained flexural loadings. The main objective of this study is to investigate the Long Term Flexural Behavior of Pre-Cracked Fiber Reinforced Beams under Sustained Loads. The experimental reports document the effect of loading and temperature on the creep characteristics of concrete. A variety of study has been carried out for the different responses generated by the creep tests based on factors like effect of temperature and humidity, effect of fiber content, effect of fiber type, and effect of different loading levels.

The Creep Testing Experimental Methodology is divided into three main parts which includes: (1) The Pre-cracking Partial Fracture Test; (2) Creep Test; (3) Post Creep Full Fracture Test. The magnitude of load applied to a specific specimen during creep

testing was based on the results of average residual strength (ARS) tests, determined using EN14651. Specimens of the synthetic FRC mixture were creep tested at loads nominally equivalent to 30% and 50% of the FR_1 value. The creep tests are usually continued until a steady Time versus CMOD response was obtained for the specimen signifying its presence in the secondary stage of creep. The creep recovery response is generated after unloading the specimen from the creep set up and later a full fracture test is carried out to obtain the complete post creep response of the beam under flexure.

The behavior of the Creep Coefficient versus Time response has been studied using various existing models like the ACI 209-R 92 Model and the CEB-FIP Model. Basic and hybrid rheological viscoelastic models have also been used in order to generate the material behavior response. A study has been developed in order to understand the applicability of various viscoelastic models for obtaining the material response of real materials. An analytical model for predicting the Flexural Behavior of FRC under sustained creep loads is presented at the end. This model helps generate the stress strain and Moment Curvature response of FRC beams when subjected to creep loads post initial cracking.

To Mumma and Papa

Who inculcated the values of perseverance, strong-will and commitment

and continually encouraged me to excel by showing immense trust in my capabilities.

ACKNOWLEDGEMENTS

Foremost, I would like to express my sincere gratitude to my advisor Dr. Barzin Mobasher, for providing me with an opportunity to work in his research group. The constant motivation, enthusiasm and patience that he has held and the invaluable insights that he has given me has always steered me in the right direction. I would also like to thank my committee members, Dr. Subramaniam D. Rajan and Dr. Narayanan Neithalath, who have supervised my progress and given me valuable comments on my work.

I would also like to specially thank Dr. Yiming Yao, who made sure I learnt all the skills essential to work on this project and patiently helped me out at every step of my work.

I am also very thankful to Mr. Peter Goguen and Mr. Jeff Long for all their help in the laboratory and the supervision of all the testing devices. I would like to thank my dear friends and colleagues, Himai, Vinodh, Jacob, Dafnik for their help in the experimental work and moral support.

Finally, I would like to express my profound gratitude to my parents, bhai-bhabhi, my baby niece and my boyfriend, who have been a major source of inspiration and have constantly supported me. Also my dear friends who helped me stay sane and motivated me throughout my Graduate School. This accomplishment wouldn't have been possible without them. Thank you.

TABLE OF CONTENTS

Page

LIST OF FIGURES

Figure Page

Figure Page

Figure Page

Figure Page

Figure Page

Figure Page

LIST OF TABLES

Table Page

1. Introduction and Literature Review of Creep

1.1 Introduction

Creep is a term used to define the tendency of materials to develop increasing strains through time when under a sustained load, thus having an increase in deflection or having an elongation with time in relation to the short-term strain [1]. Fiber reinforced concrete is a concrete that contains short discrete fibers which are uniformly distributed and randomly oriented throughout the matrix. The role of fibers is to help bridge the micro and macro cracks that form in concrete and allow for load transfer across them. Studies on creep of FRC in compression indicate that fibers restrain creep strains when compared to plain mortar and concrete [2]. Long term behavior of FRC has not been fully addressed and evaluated when concrete is in tension and cracks have occurred in them, hence the fibers are resisting the crack opening. Such a behavior has not been considered in design codes yet.

There exists literature on the long-term behavior of FRC under sustained tensile loadings. As FRC in service could be in cracked state, the serviceability and failure will depend on the stability of the cracks, and the alteration of the capacity to transfer stresses [3]. This thesis addresses the effect of loading, fiber type and temperature on the creep characteristics of a cracked fiber reinforced concrete section. The primary focus is on the developing a model that will help generate the stress strain response and the

load – crack mouth opening displacement relationship for a cracked fiber reinforced concrete specimen under sustained loads.

1.1.1 Fiber Reinforced Concrete Components and Cracking Phenomenon

Fiber Reinforced Concrete is composed of cement, aggregates, water, admixtures and short fibers that are mixed in the fresh concrete creating a random orientation and uniform distribution throughout the matrix. The fibers are well mixed thus providing a three-dimensional reinforcement throughout.

Creep is caused by many complex mechanisms that include micro-mechanisms which originate from the hardened cement paste. Portland cement paste consists of a solid gel which contains many capillary pores and is made of colloidal sheets of calcium silicate hydrates, separated by spaces containing absorbed water [4]. This mechanism is mostly evident in the compression creep of concrete. However, the experimental plan deals with the behavior of fiber reinforced concrete in tension as a crack propagates in the tension zone of the flexural loaded beam specimen. The mechanism of the crack propagation of Fiber Reinforced Concrete in the tension zone under creep is given below. Emphasis has been made on the cracked region and the fibers resisting the crack growth.

In Fiber Reinforced Concrete, the time dependent crack propagation can be attributed to two mechanism: fiber creep and gradual fiber pull out

from the concrete matrix [5]. The fibers restrain the crack propagation by taking the tension forces and transferring them across the crack faces. As the crack propagates, the fibers may be extended so much as to fiber fails in tension. A similar schematic illustration of a multi-scale fiber reinforced system has been given by Fantilli et al [6].

Figure 1: Crack propagation of fiber reinforced concrete under sustained loads

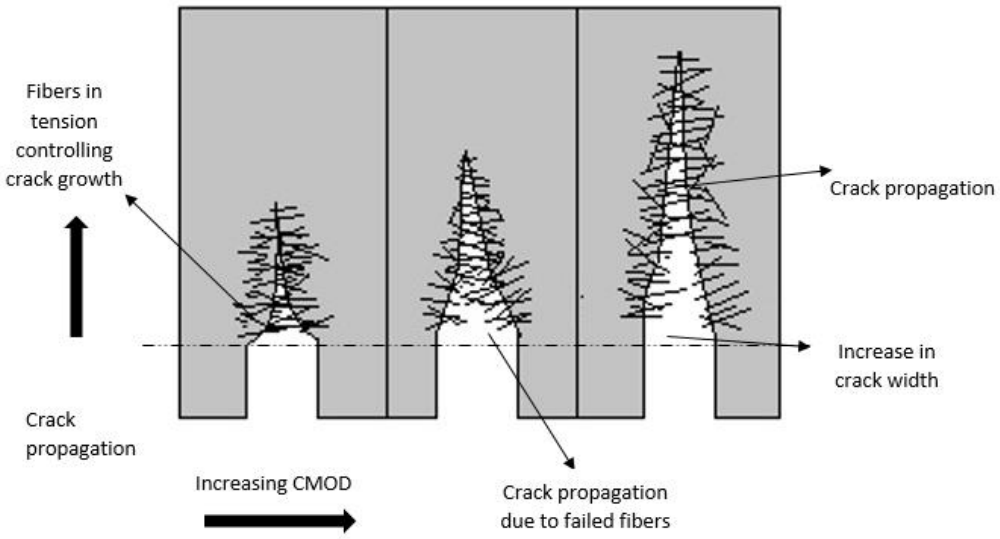

Figure 2: Fiber Matrix Interface at the various stages of loading

Figure 3: Comparative response of Fiber Reinforced Concrete and Plain Concrete under flexure

The study is directed to understanding the creep of cracked FRC and generating a comparative response of different fiber types. The main objective is to conduct post cracking creep tests on fiber reinforced concrete

(FRC). There is absence of information in literature on the time-dependent behavior of FRC under sustained loading. In order to efficiently and effectively increase the use of FRC material, the creep of FRC as a time-dependent behavior needs to be included in design guidelines. Hence, pre-cracked samples were tested at distinct levels of sustained loading to document the increase of the crack opening of tensile and flexural samples.

A summary for recent relevant research publications is presented. Burratti et al [7] presented a literature review on the main testing methodologies used to investigate the long-term behavior of cracked FRC elements. With a focus on the flexure tests, the typical behavior of FRC in softening observed when under sustained loads in a cracked condition was discussed. Figure 4 shows the complete stress versus CMOD response for a typical strain softening FRC specimen under creep.

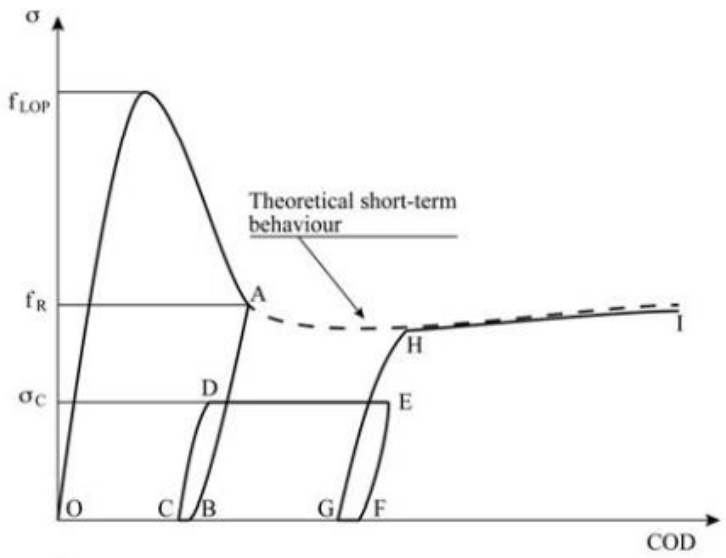

Figure 4: Stress versus CMOD relation for a typical strain softening FRC specimen [7]

Arango et al [8] proposed a test setup and methodology for testing the flexural creep behavior of pre-cracked FRC specimens. A testing procedure along with the design criteria used to define the equipment and the test methodology was presented. The test results and the models developed in the present work were used to address the experimental results of Arango et al.

Burratti et al [9] carried out a set of experiments that included procedures for pre-cracking, unloading, followed by reloading the flexural beams. The aim of the experiment was to investigate the long-term behavior of cracked steel fiber reinforced concrete beams under four-point bending loads. One specimen was exposed to drying- wetting cycles of a 5% NaCl

solution in order to address considering aggressive environmental conditions and the rest of the beams were tested in a regular manner.

In addition to the crack mouth opening displacement, the mid span displacement of the beams was also measured by Burratti. Full fracture tests were conducted on the specimens at the end of the creep tests. The geometry of the steel fibers used to reinforce the specimen are shown in the Figure 5.

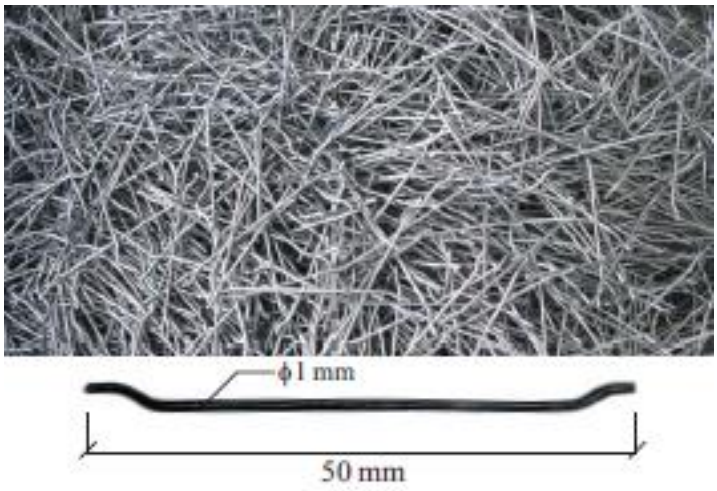

Figure 5: Steel Fibers used as Fiber Reinforcement and its Geometry [9]

Tests demonstrating the effects of fiber types and fiber dosage were carried out by Bergen et al [10] to demonstrate the long term behavior of cracked fiber reinforced concrete under sustained loads. MacKay and Trottier [11] described the results of experimental tests comparing the behavior of one steel fiber reinforced concrete and one type of polymeric fiber reinforced concrete under long term sustained loading.

Kurtz et. al. [12] carried out the experimental investigation of the creep-time behavior of fiber reinforced concrete with polypropylene and nylon fibers. The experimental plan consisted of testing the beams for various stress levels to observe three different experimental outcomes: load sustained indefinitely (low stress), creep failure (intermediate stress), and rapid failure (high stress). The maximum flexural stress that can be applied indefinitely without failure was determined. Kohoutkova et al [13] presented a model for creep and shrinkage of Fiber Reinforced Concrete. The model considers the influence of factors that include fiber type, shape, and interface fiber-matrix-bond.

1.2 Experimental Procedures

Experimental plans with similar end goals and varying experimental set-ups were adopted in different research projects. The test set up developed by Arango et al [14] consisted of three important components which are the creep frame, the measuring devices and the Data Acquisition System (DAS). A gravity loading system was used to apply loads on the test specimen. A set of elements were designed so as to apply the load and to support the test specimen designed. The tests were carried out in controlled environment. The schematic of the test setup used by Arango is shown in figure 6.

The humidity and the temperature controlled creep tests were carried out at a constant relative humidity of 50% and a temperature of 20℃ for all specimen.

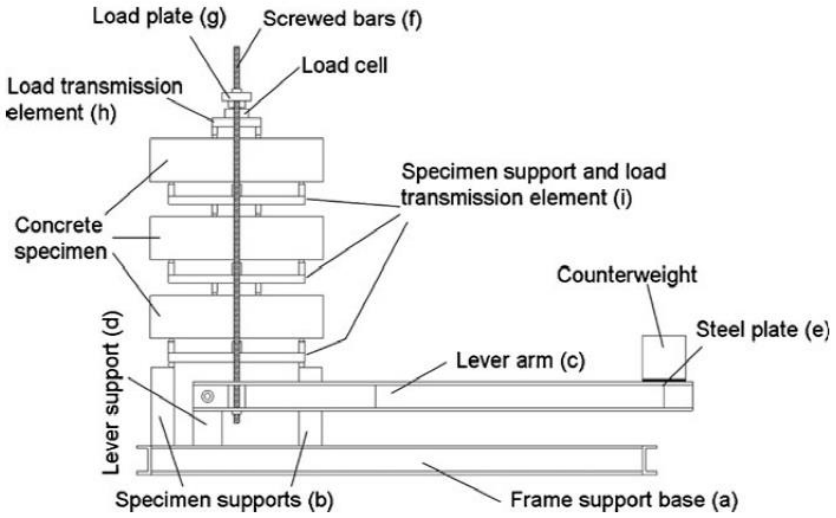

Figure 6: Schematic of the test setup used by Arango et al. [14]

The present thesis adopted an approach similar to the experimental plan by Burratti. In their tests, the beams were pre cracked up to 0.5 mm which is the upper limit of the crack width of concrete pavement at serviceability limit state before the creep tests. In order to obtain a more stable fracture process and a better control on the crack width, a steel beam was laid upon each concrete beam. Differentiating the behavior of the steel beam from that of concrete posed as a difficulty because of the method adopted to obtain stability in the fracture process. With varying crack widths

obtained at the end of the pre-cracking process, the tests were declared unstable.

The magnitude of the load corresponding to the creep loading was determined in the following manner. Notched beams were subjected to bending tests until a CMOD corresponding to 0.55mm. The load value that corresponded to a nominal stress value at the mid-span equal to 50% of the average value of the flexural stresses was calculated.

For the long term test set up, the beam specimen was sustained by two steel trestles at intermediate supports as shown in figure 7. The dead loads were applied at the beam extremities using steel plates. The set up was laid on steel supporting system which consisted of a base plate and a four point bending scheme was adopted.

Figure 7: Creep Testing Set-up used by Buratti et al [**Error! Bookmark not defined.**]

An optical device was used to measure the crack width openings, while a LVDT was used to measure the mid-span deflection. The climate controlled room for the experimental plan had a constant temperature of 20°C and a Relative Humidity was maintained at 60%.

The specimen used in the experimental approach by Kurtz et. al. [15] had two different types of polymeric fibers which were polypropylene and nylon fibers. The former were fibrillated type of fibers while the latter were a single filament kind of fiber. The mix proportion for producing the test specimen is given below:

Table 1: Mix Design Proportions used by Kurtz et al

Component	**Proportion (kg/m^3)**
Portland Cement	340
Fine Aggregate	804
Course Aggregate	1033
Water	130
Air Entraining Admixture	0.13
High Range Water Reducing Admixture	10.77
Fibers	0.9

The fiber dosage of both polypropylene and nylon 6 fibers had a volume fraction of 0.10% and 0.08% for polypropylene and nylon 6 fibers respectively in order to generate typical field usage conditions for the test

specimen. Twelve beams were cast for each fiber type of specimen with a standard size of 4x4x14 inches, which were smaller than the specimens used for the experimental plan. Five sample cylinders were cast for each specimen type to test for the compressive strength of the concrete. The beams and cylinders were cured for 27 days with 70° F temperature and 100% humidity. The test procedure used for carrying out the flexural test was as given in the ASTM standard C 1399 [16]. The pre-cracking of the beams was carried out by a deflection control method in order to minimize the fracture damage. The beams were pre-cracked by supporting them using a steel plate like the experimental set-up used by Buratti et al [11]. The test set up as described by ASTM has been given below.

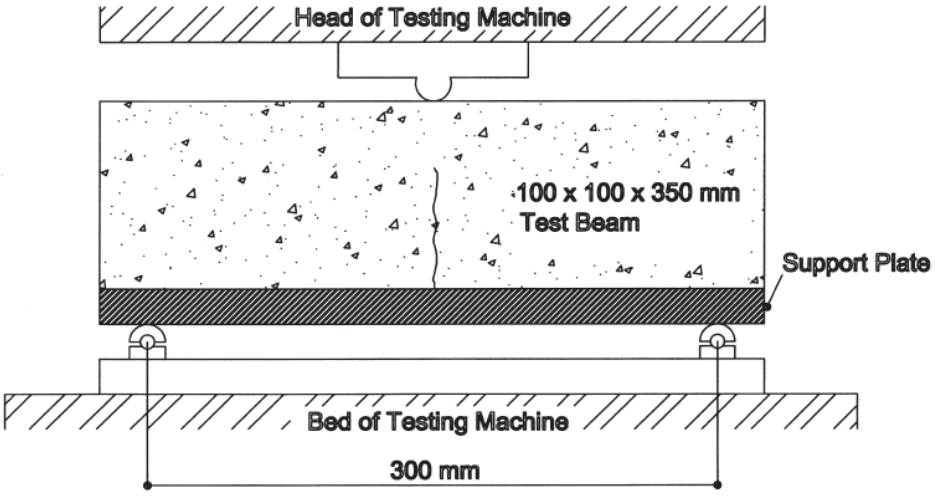

Figure 8: ASTM C 1399 Pre-Cracking Test Set-up [16]

After the pre-cracking procedure was carried out for all the twenty-four specimens, two beams of each specimen type were loaded in four point

bending test until failure. Dial gauges were used and the load and deflection values were manually noted down every 0.127 mm. The calculations of the average residual strength were carried out using the ASTM Standard formula.

The creep tests on the pre-cracked beams were performed in temperature and moisture controlled room. A temperature and relative humidity of 20°C and 50% respectively were maintained in the testing room. The creep tests were continued until a displacement of 0.75 mm was obtained for each specimen. The service load subjected on the specimens ranged from 22% to 88% of the average residual strength (ARS).

The reading for this test was taken every minute for the first hour, every hour for the next 24 hours and later just once in 4-8 hours till the end of the tests. The deflection was measured in the number of rotations of the dial gauge.

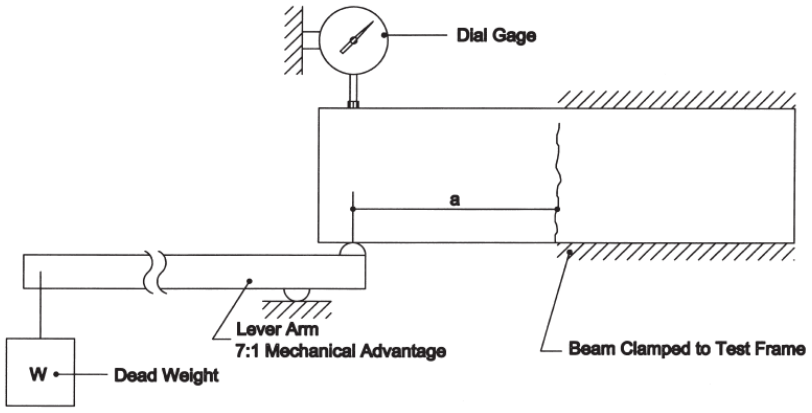

Figure 9: Creep Test Set-up as used by S. Kurtz et. al. [12]

1.3. Stages of Creep response

The deformation due to creep can be differentiated in three distinct stages as given below:

- Primary Creep
- Secondary Creep
- Tertiary Creep

Methods of predicting the primary and the secondary creep have been discussed. The strain rate is very high in the primary stage and the sample is reacting to the sudden change in the load as the time increases the strain rate decreases until it becomes almost zero. Secondary creep is the dominant stage in the entire span of creep, where most of the creep deformations takes place which is not reversible and for most of the part it is characterized by the linear increase of strain with time. The tertiary creep stage comes into picture when the creep rate increases as a function of time to an ever increasing deformation rate. This behavior normally leads to creep failure as the same is about to fail and the strain rate starts increasing exponentially. The tertiary creep stage involves development of a steep spike in the creep response curve after leaving the secondary stage.

1.3.1 Case Study of Tertiary Creep

Stewart et al [17] discussed the basic mechanism for creep for NI-base super alloys that include the diffusion flow, dislocation slip and climb,

and grain boundary sliding. A basic graph to indicate the behavior of the super alloy was expressed as given below:

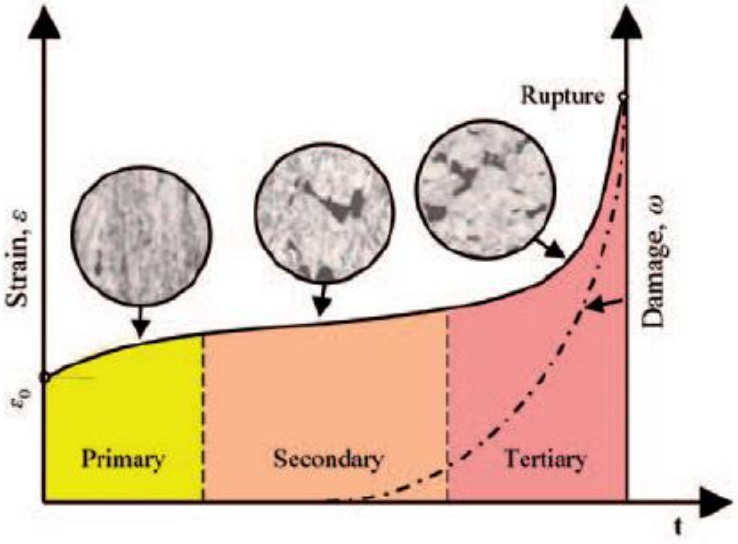

Figure 10: Creep Deformation and Damage Evolution [17]

Figure 10 shows a model to put the three regions of creep in perspective. Note that it is possible to introduce a parameter of damage as a variable in the model.

The primary and secondary creep parameters can be obtained using standard spring – dashpot models which can be calibrated for various experimental data. A series of these models have been developed and applied to the experimental data of this study

An approach to determine the tertiary creep-damage constants analytically from experimental data was developed by Stewart et al [17]. For developing this approach and obtaining the tertiary creep-damage

constants, strain-based and damage-based approach were exercised. Mathematically, the tertiary creep-damage constants were determined analytically in two ways:

- Strain Approach (SA) - where the damage evolution equation is incorporated into the creep strain rate equation.
- Damage Approach (DA) – where the available creep strain rate data are used to approximate the damage evolution.

These approaches were used to generate the simulation results for the experimental data later.

2. Experimental approach to Flexural Creep Testing of Partially Cracked FRC Beams

2.1 Introduction

This section discusses the various components of a flexural creep testing system. The components of the test set up in the various phases in addition to the test procedures, the data acquisition, and data processing are explained in detail. The various phases of the complete procedure of the creep testing includes the casting and curing of specimens, the partial fracture tests, the flexural creep tests and the full fracture tests. Each apparatus has been described in detail below.

Several types and geometries of fibers can be used for reinforcement. The fiber types that were used in this project for addressing the flexural creep experiments were two types of polymeric fibers and steel fibers with hooked ends. The pictures of the steel and the polymeric fibers labelled as Polymeric Fiber Type 1 and Polymeric Fiber Type 2 are given in figure 11:

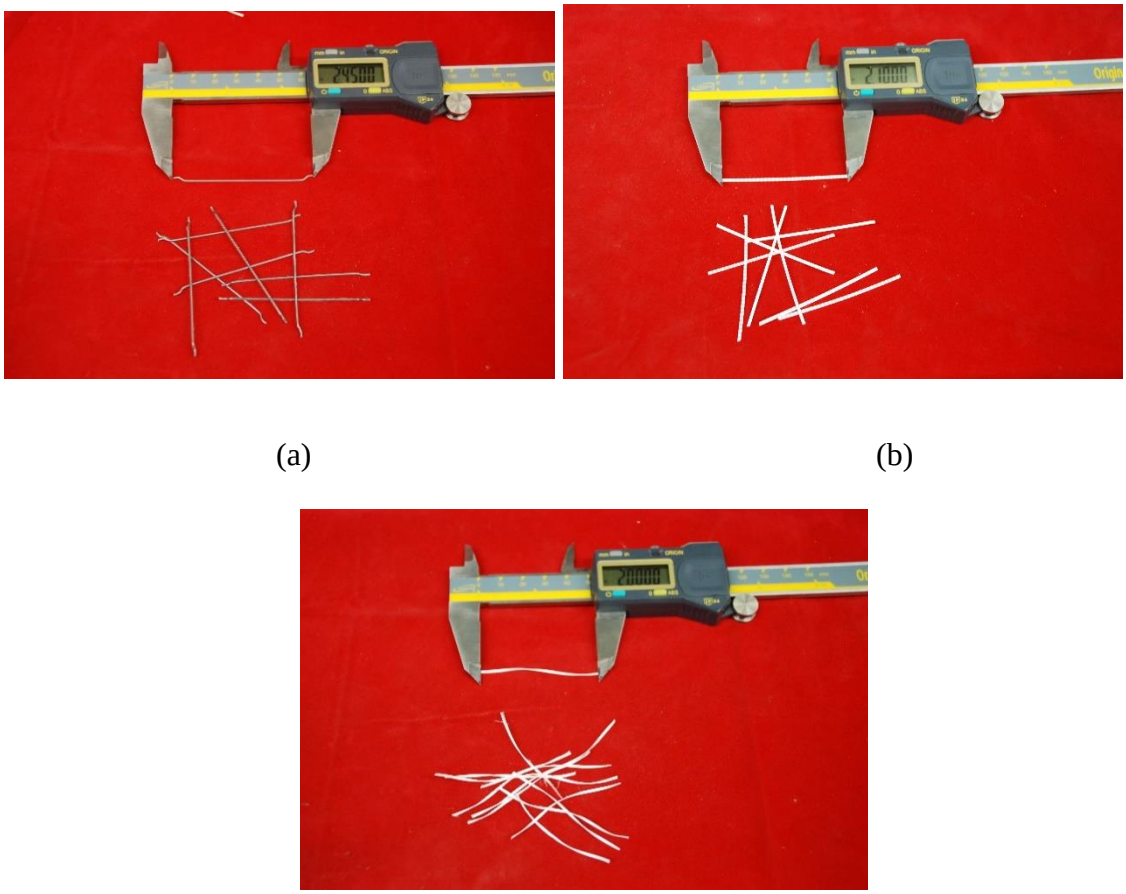

(a) (b)

(c)

Figure 11: Different fibers used for the experimental plan: (a) Steel Fibers, (b) Polymeric Fiber Type 1, (c) Polymeric Fiber Type 2

The steel fibers used for the experimental plan had a length of 35 mm each with hooked ends and a fiber diameter of 0.55mm. The tensile strength of the steel fiber used was 1.345 N/mm^2. The type 1 polymeric fibers have a rectangular cross section with a cross sectional dimension of 0.5x1.2mm and an equivalent diameter of 0.89mm. Each fiber is 54mm long with a

tensile strength of 585 MPa. The type 2 polymeric fiber has a length of 51mm with a tensile strength varying from 600-650 MPa.

2.2 Experimental Set-up and Test Methodology

2.2.1 Flexural Creep Testing Equipment

For the experimental plan, six different sets of flexural creep testing systems were built based on three 20-ton hydraulic press frames. Each frame was utilized in a way to test two beams in parallel. Air pressurized pistons were used to apply the required load on the beams. Figure 12 and Figure 13 presents the schematic drawing and images of the components.

Different beam specimens with varying strengths were tested in the experimental plan which involved varying load levels on each specimen. Four sets of the systems were equipped with high capacity pistons (up to 10,000 lbs.) on two of the frames and low capacity pistons (up to 2,000 lbs.) were employed on two systems as shown in Figure 12. However, in the phase 3 of experimental plan the low capacity piston was replaced with the high capacity piston.

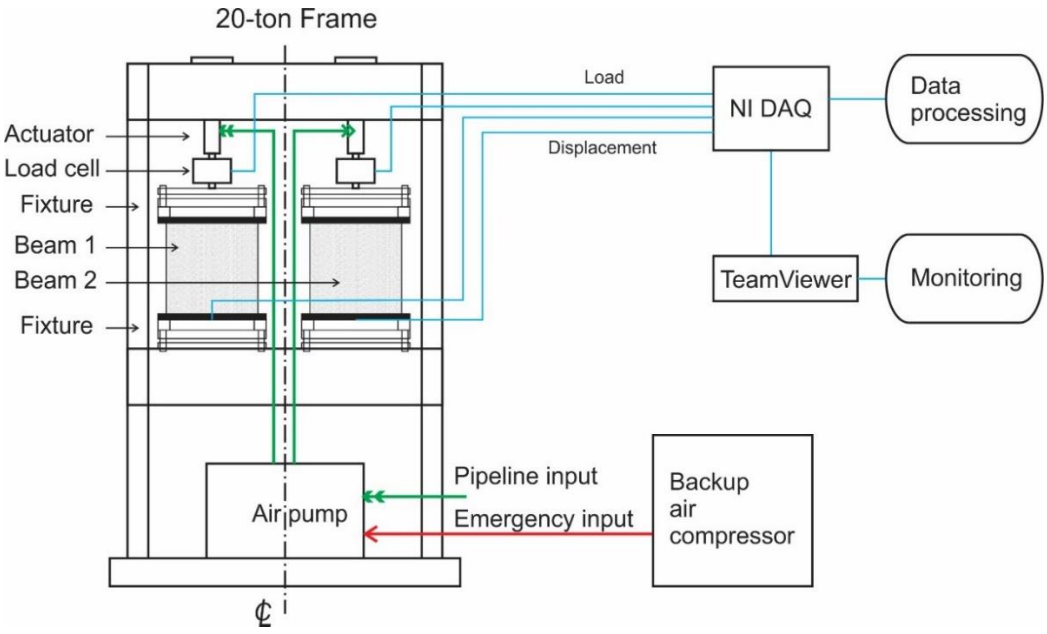

Figure 12: Schematic Drawing of the Testing System

For monitoring the experimental results, the load and the Crack Mouth Opening Displacement (CMOD) data were acquired using a National Instruments data acquisition system through LabVIEW VI programs. Also, as different specimen were tested at varying levels of humidity and temperatures, a testing room was constructed to control the humidity and the temperature using heat lamps and humidifiers as shown in Figure 15.

(a)

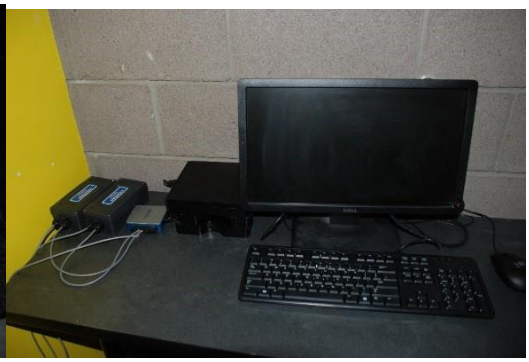

(b)

(c)

Figure 13: (a) Air Pump, (b) NI DAQ and Computer and (c) Back Up Air Compressor

(a) (b)

Figure 14: (a) Testing Frame with High Capacity Piston, (b) Testing Frame with Low Capacity Piston

2.2.2 MTS Test Machine

Before placing the beams on the creep testing frames, partial fracture tests were carried out on the notched beams using the MTS machine as shown in Figure 16. The beams were notched right at the center of the span and the loading head is aligned to the notch. This correct alignment of the specimen was ensured by using a laser alignment mechanism. Testing jig was mounted at the center of the face of the beam on each side, to which

one LVDT was attached to measure the axial deflection at the mid-span. The extensometer used as a feedback for controlling this test was mounted near the notch using multiple metal plates. Another LVDT was placed at the bottom of the specimen along the notch to measure the CMOD up to about 7 mm of crack width opening.

(a) (b)

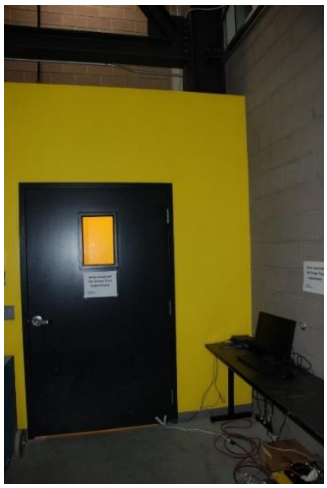

(c)

Figure 15: (a) Heat Lamp, (b) Humidifier, (c) Temperature and Humidity controlled Testing Room

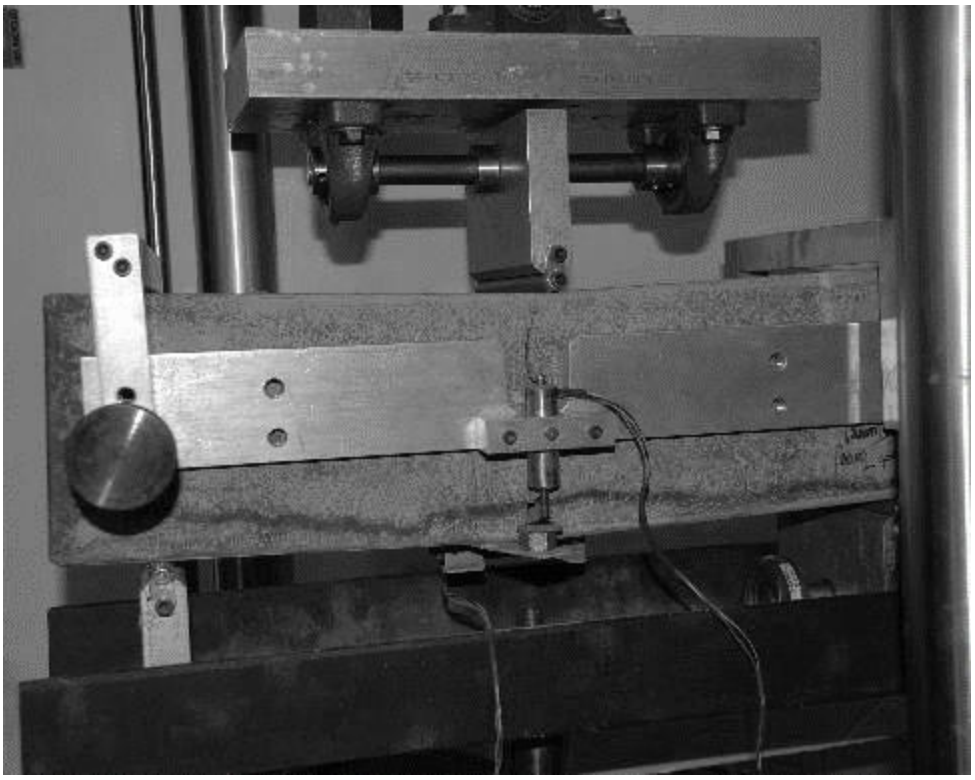

Figure 16: Experimental Setup used for running the monotonic fracture tests

The magnitude of load applied to a specific specimen during creep testing was based on the results of average residual strength (ARS) tests, determined using EN14651 [18]. Specimens of the synthetic FRC mixture were creep tested at loads nominally equivalent to 30% and 50% of the FR_1 value.

2.3 Compression Tests Results

Compressive strengths of 4 x 8 inches' cylinders from two batches B2, B3, B4, B5 & B6 were tested at a loading rate of 400 lbf/s (according to ASTM C39). Test conducted on 7, 14, 28 and 56 days of curing are summarized in Table 2 & Table 3.

Figure 17: Concrete Cylinder after compression failure

Table 2: Compressive Strength of the 4x8 cylinder specimens of Phase II (Polymeric fiber type 1)

Fiber Content	Specimen	Days	Compressive Strength (psi)
7.5 pcy	1	7	3444
	2	7	3195
	3	14	3722
	4	14	3976
	5	28	4468
	6	28	4799
	7	56	4920
	8	56	5278
10 pcy	1	7	3536
	2	7	3524
	3	14	3988
	4	14	4139
	5	28	4144
	6	28	4702
	7	56	5261

	8	56	5234
15.3 pcy	1	7	5925
	2	7	6013
	3	14	6680
	4	14	6660
	5	28	7562
	6	28	6876
	7	56	8364
	8	56	8006

Table 3: Compressive Strength of the 4x8 cylinder specimens of Phase III

Fiber Type	Specimen	Days	Compressive Strength (psi)
Polymeric Fiber Type 1	1	7	8380
	2	7	8356
	3	14	9302
	4	14	9414
	5	28	10130
	6	28	9931
	7	56	11714
	8	56	12446
Steel	1	7	8356
	2	7	8108
	3	14	8371
	4	14	8825
	5	28	8817
	6	28	8658

	7	56	12684
	8	56	12772
Polymeric Fiber Type 2	1	7	8809
	2	7	7513
	3	14	8801
	4	14	8172
	5	28	9573
	6	28	9525
	7	56	12310
	8	56	12286

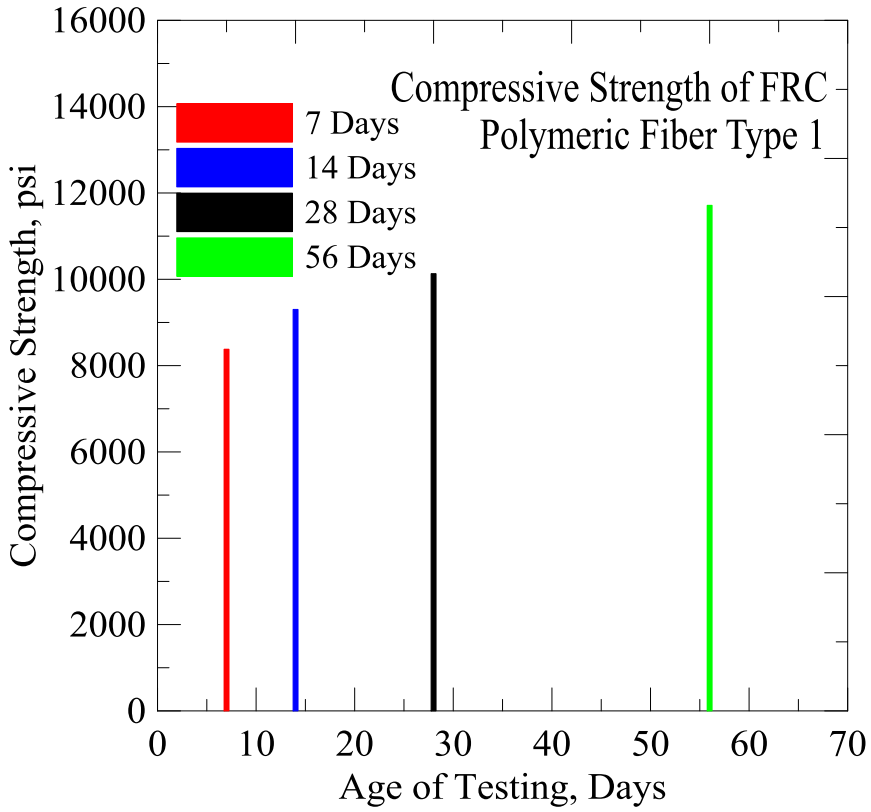

Figure 18: Comparative compressive strength plot for concrete cylinders

2.4 Creep Testing Methodology

The following procedure was adopted for testing cracked beam specimens for flexural creep response.

1. The first step involves the partial flexural test or the controlled flexural test. The Fiber Reinforced Beam Specimen were loaded under monotonic closed loop of a CMOD controlled flexural test on the MTS machine up to a CMOD value of 0.05mm i.e. 0.02 inch, according to RILEM TC 162 and the corresponding fracture load was recorded.
2. As soon as the required CMOD value was achieved, the test was paused and the sample was unloaded.
3. The specimens were then transferred to the creep frame and loaded again with the required service load, usually the 30% or maximum load.
4. The flexural deformation due to the service load was continuously monitored under the sustained loading for about 70-90 days using the CMOD value.
5. Load and CMOD data were monitored throughout the creep loading phase.
6. The specimens were tested for about 70-90 days and then the test was stopped and the beams were unloaded.

7. The CMOD values of the specimen were then checked after about a week in order to know the recovery made, if any.
8. Full fracture tests were run on the specimens tested for creep to obtain the post creep response under loading.

2.4.1 Experimentation Summary

A – Type of Concrete, 1=NSC, 2=HPC

B I-VI –Mix Design of the batches which are shown in Table 4.

R - Service load applied to the beams, 30=30%, 50=50%

D - Days cured in the curing chamber

S – Specimen

(Example: A1_B4_D14_R50_S1 means **S**pecimen 1 of Normal Strength Concrete beam casted out of Batch 4 which was cured for 14 days loaded in the creep frame at 50% of FR1.)

Table 4: Summary and Notations

Phase	Series	A	B	R	D	S	ID	Note
II	4	NSC	IV	50	14	1	A1_B4_D14_R50_S1	
				50		2	A1_B4_D14_R50_S2	
				-		3	A1_B4_D14_S3	Full Fracture
				-		4	A1_B4_D14_S4	Full Fracture
	5	NSC	IV	50	14	1	A1_B5_D14_R50_S1	
				50		2	A1_B5_D14_R50_S2	
				-		3	A1_B5_D14_S3	Full Fracture
				-		4	A1_B5_D14_S4	Full Fracture

	6	HSC	VI	50	14	1	A2_B6_D14_R50_S1	
				50		2	A2_B6_D14_R50_S2	
				-		3	A2_B6_D14_S3	Full Fracture
				-		4	A2_B6_D14_S4	Full Fracture
III	4	HSC	VI	50	14	1	A1_B7_D14_R50_S1	
				50		2	A1_B7_D14_ R50_S2	
				-		3	A1_B7_D14_S3	Full fracture
				-		4	A1_B7_D14_S4	Full fracture
	5	HSC	VI	50	14	1	A1_B8_D14_R50_S1	
				50		2	A1_B8_D14_R50_S2	
				-		3	A1_B8_D14_S3	Full fracture
				-		4	A1_B8_D14_S4	Full fracture
	6	HSC	VI	-	14	1	A2_B9_D14 _S1	Full fracture
				50		2	A2_B9_D14_R50_S2	
				50		3	A2_B9_D14_R50_S3	
				-		4	A2_B9_D14_S4	Full fracture

2.4.2 Experimental Protocol Verification

Before getting started with the tests, a trail batch was tested according to the procedures so as to verify if the experiment would run successfully. For the same, six beams of 6x6x22 inches were cast with the polymeric fiber type 1 using the mix design as shown in Table 5. For this set of specimens,

one of the beam was tested for fracture load test, whereas creep testing was carried out on 5 other specimen at R30 and R50 to verify the testing equipment as given in Table 6.

Table 5: Mix Design for Trial Batch (B1)

Ingredients	NSC
	Batch Weight , lbs. cubic yard
Cement	643
Sand	1400
#57	1006
#8	612
Fiber (POLYMERIC FIBER TYPE 1)	5
Water	482

Table 6: Testing Matrix for Trial Batch

S	No. of Days Cured	Service Load applied (% of F_{R1})
1	7	50
2	30	50
3	30	50
4	30	30
5	30	30
6	30	Full fracture test

The initial trial run for creep test with the specimen S1 was performed for 33 days under the service load of 680 lbf, which was basically the 50% service load. After the completion of this test it was observed that there was no flexural failure observed and the CMOD values increased from 0.02 inch to 0.133 inch in the test span. Thus it was be concluded that a higher service load i.e. a service load greater than 50% would be required for the creep failure of the beam in flexure. Post testing the beam and the load and CMOD responses looked as given below in Figure 19:

(a)

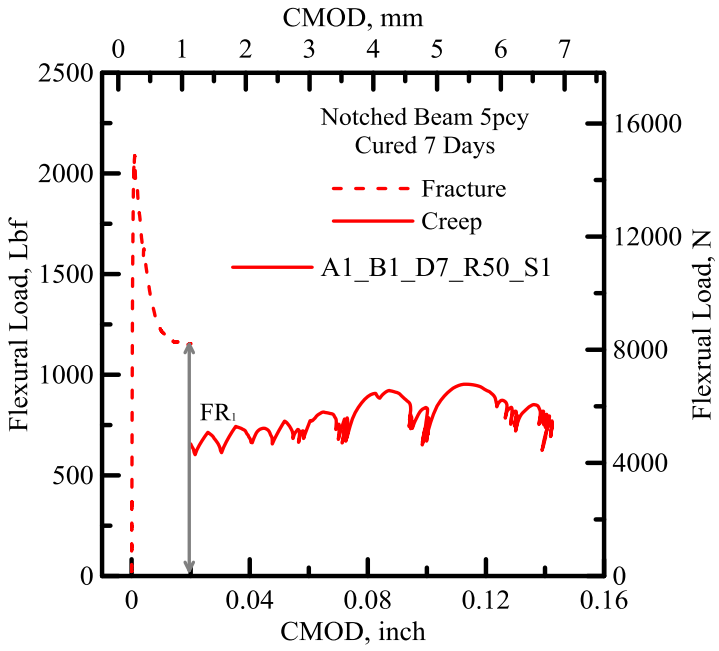

(b)

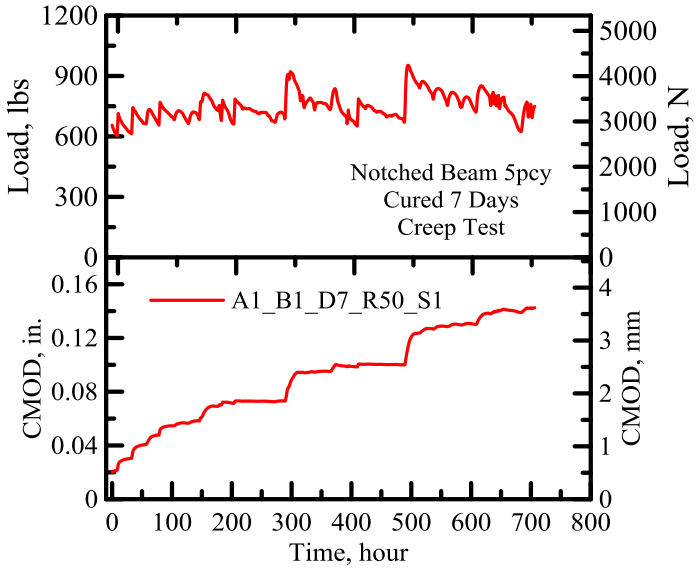

(c)

Figure 19: (a) Specimen 1 post testing, (b) Load vs CMOD plots for both fracture and Creep tests, (c) load and CMOD vs time history plots of the creep test

After the creep tests were carried out for all the specimen the following data was found and it was concluded that service load of 30% would not be enough for the crack propagation as compared to the R50 load.

Table 7: CMOD values for Trial Beam Specimen

S	FR_1(inches)	CMOD (inches)	No. of days cured	Flexural Failure	Day of Failure
1	0.02	0.131	7	No	-
2		0.107	30	No	-
3		0.243	30	Yes	16
4		0.017	30	No	-
5		0.017	30	No	-

2.5 Creep Experiment Phase Two

2.5.1 Mix Design

According to the preliminary study and the phase 1 of the creep experiment, two batches of specimens, both reinforced by polymeric fiber type 1 were cast at ASU using the mix design summarized in Table 8. Different slumps were obtained for both batches which was 4.5 inch and 5.75 inch using the superplasticizer – Glenium 3030 NS. It was observed that a minor variation in the addition of the admixture caused a major difference in the slump of the concrete. The creep experiments were carried out after curing these samples for 14 days in the Curing Room Facility at ASU, at a 50% service load of the FR_1. The table 8 given below gives us

the details of the mix design, whereas the Table 9 shows us the testing matrix for this phase of experiments for each batch.

Table 8: Mix Design for Phase 2

Ingredients	B4,	B5	B6
	Batch Weight , lbs. per cubic yard		
Cement	641	641	641
Sand	1352	1352	1344
#57	910	910	910
#8	739	739	739
Water	301	301	301
Glenium 3030 NS	6.8 oz/cwt	6.8 oz/cwt	7oz/cwt
Polymeric fiber type 1	7.5	10	15.3

Table 9: Testing Matrix for Phase 2 Specimen

S	No. of Days Cured	Service Load applied (% of F_{R1})	
		B4, B5	B6
1	14	50	50
2	14	50	50
3	14	Full fracture test	Full fracture test
4	14	Full fracture test	Full fracture test

2.5.2 Fracture Tests

Full fracture tests were run on the Specimen 3 and 4 for each beam type. The full fracture response for each specimen type with different fiber content has been given below. Specimens 3 and 4 of A1_B4_D14 have 7.5

pcy fiber, A1_B5_D14 have 10 pcy fiber, whereas A2_B6_D14 have 15.3 pcy fiber.

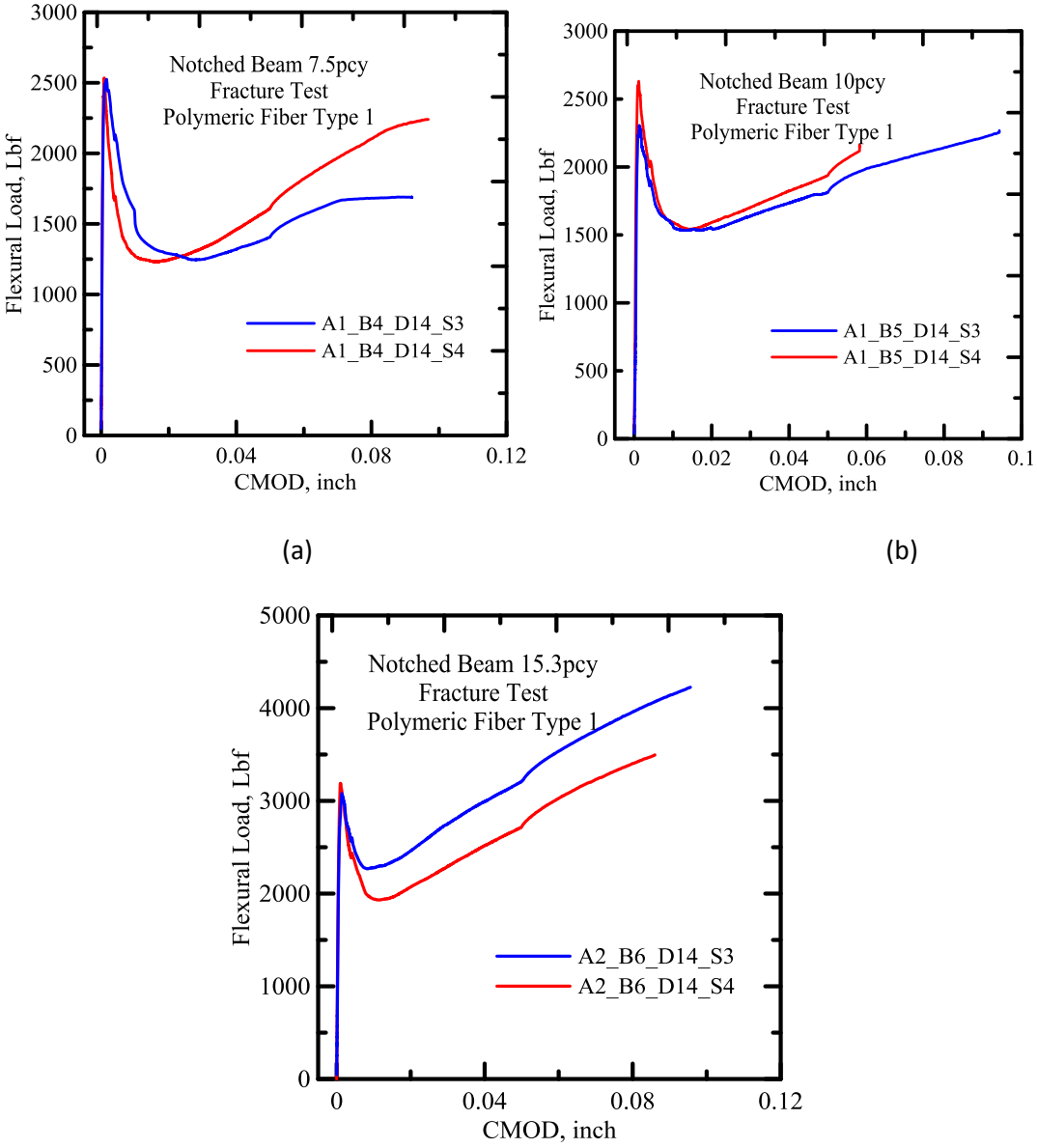

Figure 20: Responses for Specimen 3 and 4 tested for full fracture test of: (a) 7.5 pcy Fiber, (b) 10 pcy Fiber, (c) 15.3 pcy Fiber

2.5.3 Creep Tests

Two specimens of all three specimen type were first loaded under the monotonic closed loop of a CMOD controlled flexural test on the MTS machine up to a CMOD value of 0.05mm i.e. 0.02 inch. Once this CMOD value was achieved, the beams were unloaded and then placed on the creep testing frames. As the FR_1 values for each beam varied the Specimen 2 of B5 was loaded with S1 of B4 and vice versa. All the beams were loaded to 50% service load of FR_1. The plots obtained at the end of the testing phase which was around 70 days are given below in Figure 21, 22 and 23 respectively.

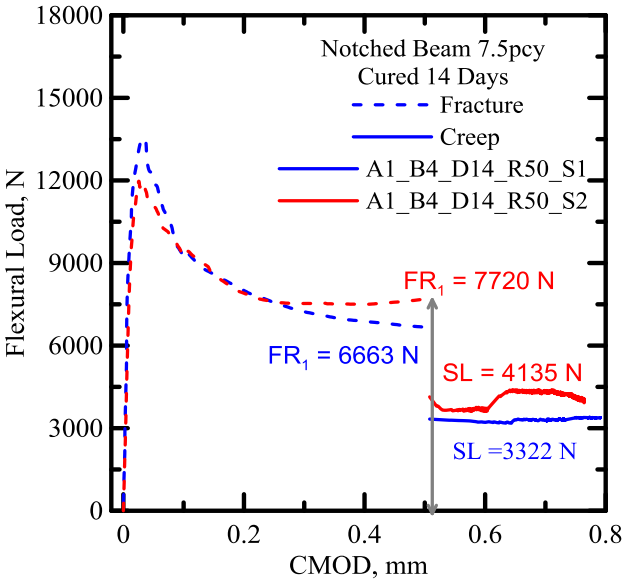

(a)

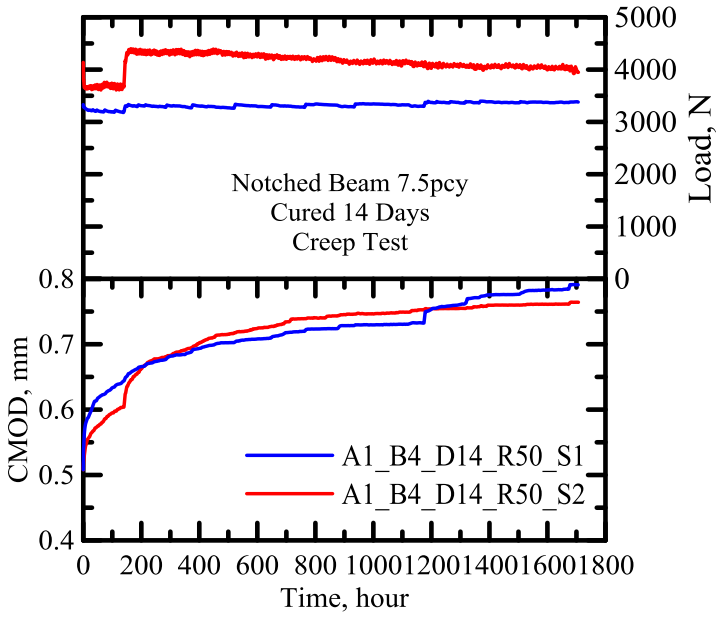

(b)

Figure 21: Responses for Specimen 1 & 2 for 7.5 pcy Fiber Content, (a) Load CMOD Curves for both Fracture and Creep Tests, (b) Load and CMOD vs Time Histories of Creep Test

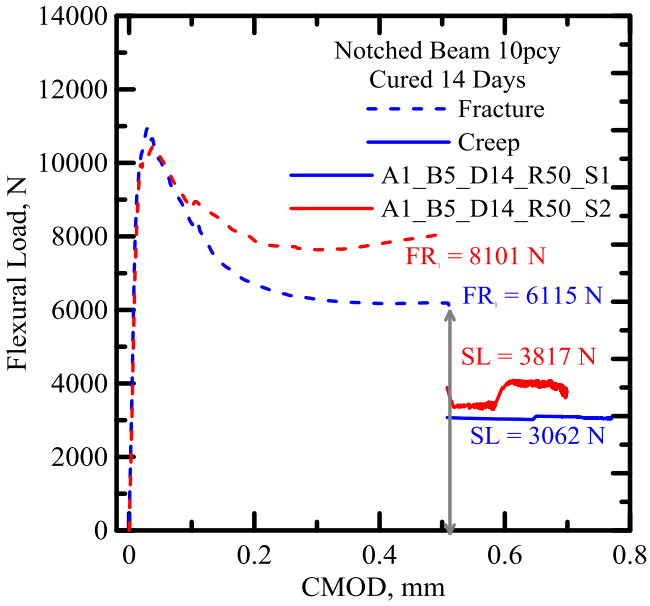

(a)

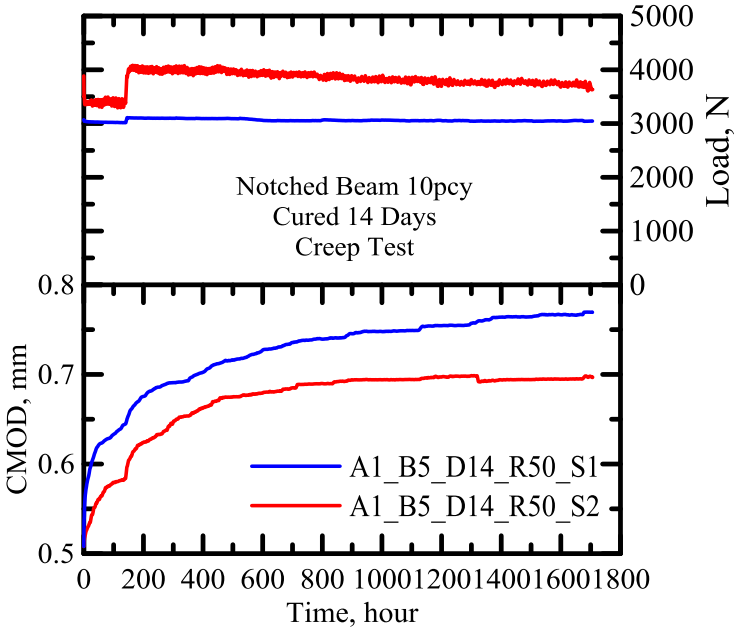

(b)

Figure 22: Responses for Specimen 1 & 2 for 10 pcy Fiber Content, (a) Load CMOD Curves for both Fracture and Creep Tests, (b) Load and CMOD vs Time Histories of Creep Test

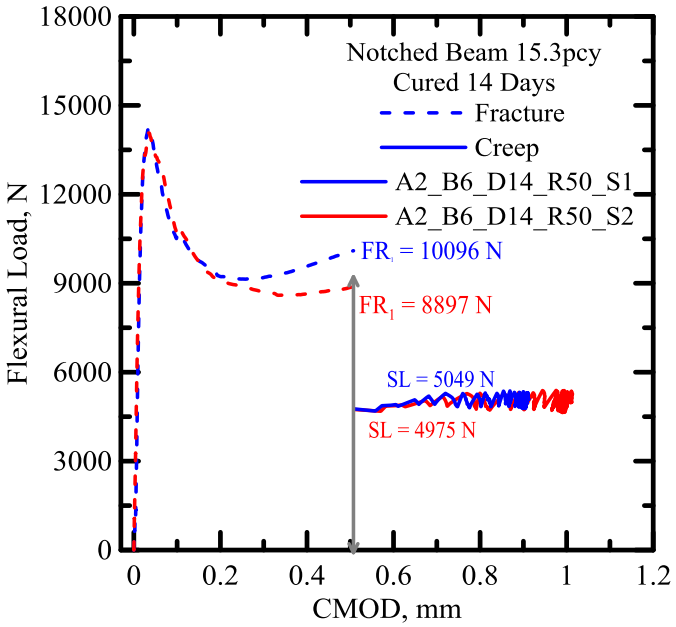

(a)

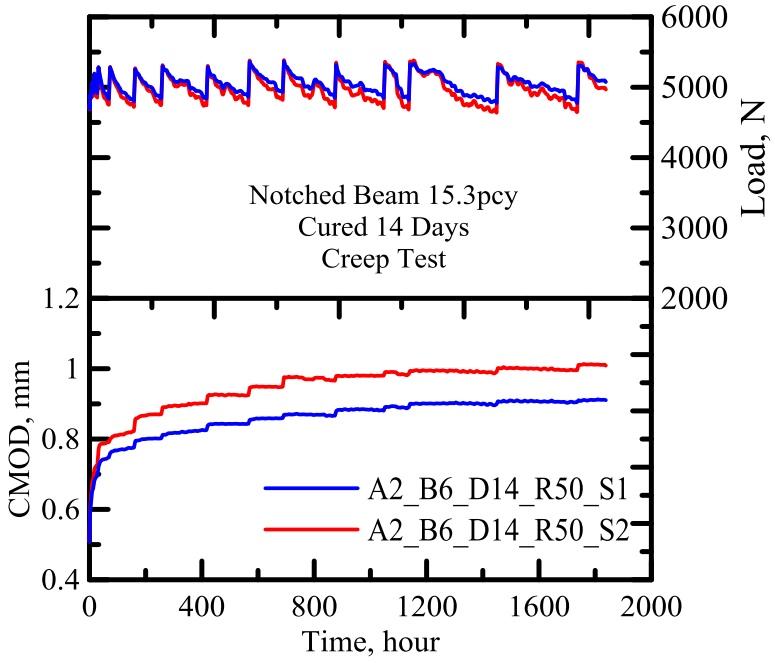

(b)

Figure 23: Responses for Specimen 1 & 2 for 15.3 pcy Fiber Content, (a) Load CMOD Curves for both Fracture and Creep Tests, (b) Load and CMOD vs Time Histories of Creep Test

Table 10: Data Results Post Creep Testing

Fiber Content	Conc. Type	S	R	Avg. Service	CMOD (mm)	CMOD (in)	Age (hours)	Flexural Failure	FR1
7.5	NSC	1	50%	3322	0.2833	0.0112	1705.99	No	6662.6
7.5	NSC	2		4135	0.2564	0.0101	1705.99	No	7719.5
10	NSC	1		3062	0.2616	0.0103	1705.99	No	6114.8
10	NSC	2		3817	0.1907	0.0075	1705.99	No	8100.8
15.3	HSC	1		5049	0.4050	0.0159	1838.01	No	10096.2
15.3	HSC	2		4975	0.5054	0.0199	1838.01	No	8896.8

2.6 Creep Experiment Phase Three

2.6.1 Mix Design

As the preliminary study, three batches of specimens reinforced by polymeric fiber type 1, steel fibers and polymeric fiber type 2 were cast at ASU using the mix design summarized in Table 11. Slump of 4.5" and 5.75" were obtained for both mixes using the amount of superplasticizer (SAP) given in the table. Creep test was done after 14 days of curing at R50 for six beams as given in the table below.

Table 11: Mix Design for Phase 3

Fiber	1	2	3
Cement I/II (lb/yd3)	624	624	624
Fly Ash - Class F (lb/yd3)	142	142	142
#57 Stone (lb/yd3)	0	0	0
#8 Stone (lb/yd3)	1259	1259	1259
Sand (lb/yd3)	1601	1601	1601
Fiber	Polymeric Fiber Type 1	Steel Fibers	Polymeric Fiber Type 2
Fiber dosage (lb/yd^3)	15.3	66	15.3
Master Glenium 7500 (oz/cwt)	25.8	25.8	47.6
Slump (in.)	8	10	3.75

Table 12: Testing Matrix

S	No. of Days Cured	Service Load applied (% of F_{R1})		
		Polymeric Fiber Type 1	Steel Fibers	Polymeric Fiber Type 2
1	14	50	50	50
2	14	50	50	50
3	14	Full fracture test	Full fracture test	Full fracture test
4	14	Full fracture test	Full fracture test	Full fracture test

2.6.2 Fracture Tests

Full Fracture tests were run on the Specimen 3 and 4 for each beam type. The full fracture response for the specimens with different fiber types have been given below.

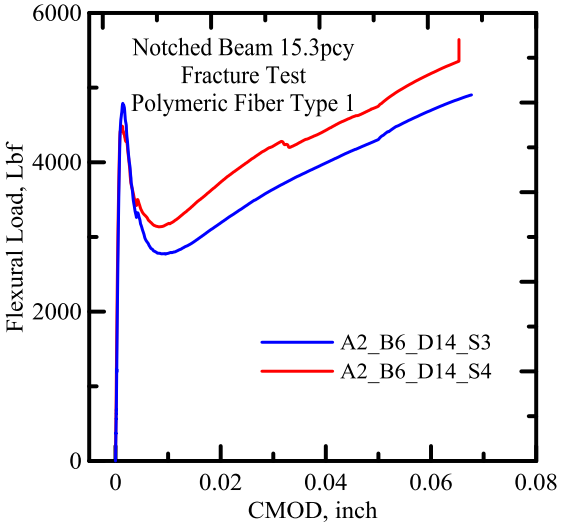

(a)

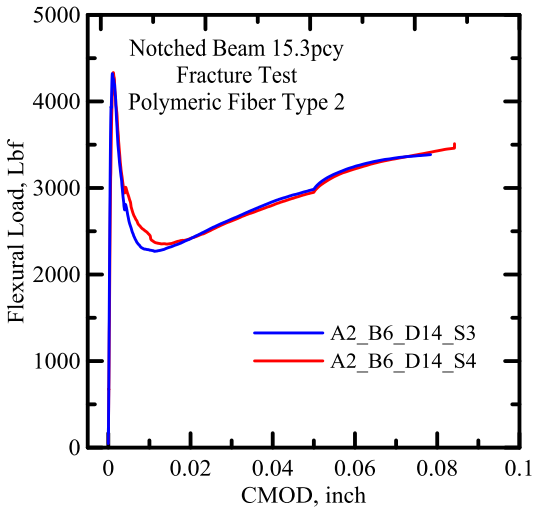

(b)

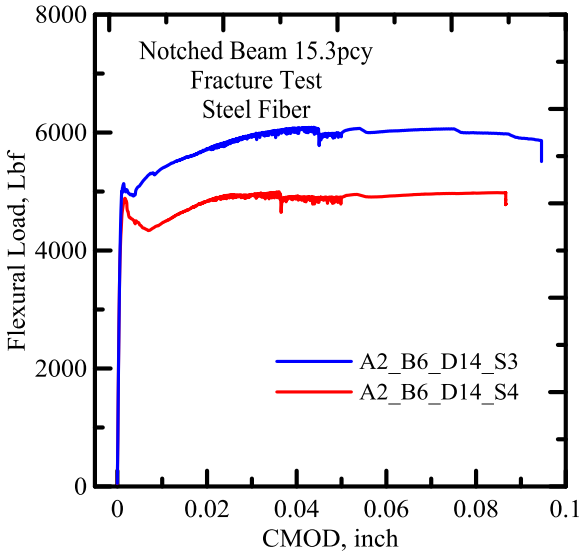

Figure 24: Responses for Specimen 3 and 4 tested for full fracture test of: (a) Polymeric Fiber Type 1 Fiber, (b) Polymeric Fiber Type 2 Fiber, (c) Steel Fiber

2.5.3 Creep Tests

The plots obtained at the end of the creep testing phase 3 which was around 70 days are given below in Figure 25, 26 and 27 respectively.

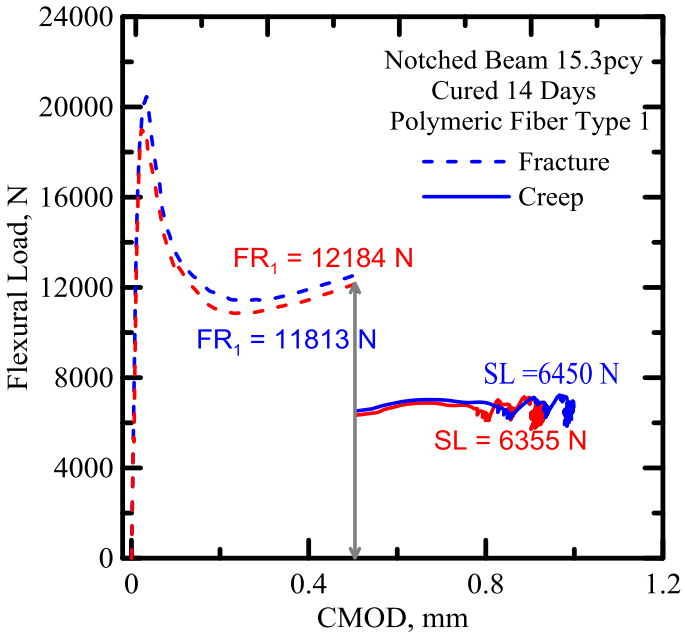

(a)

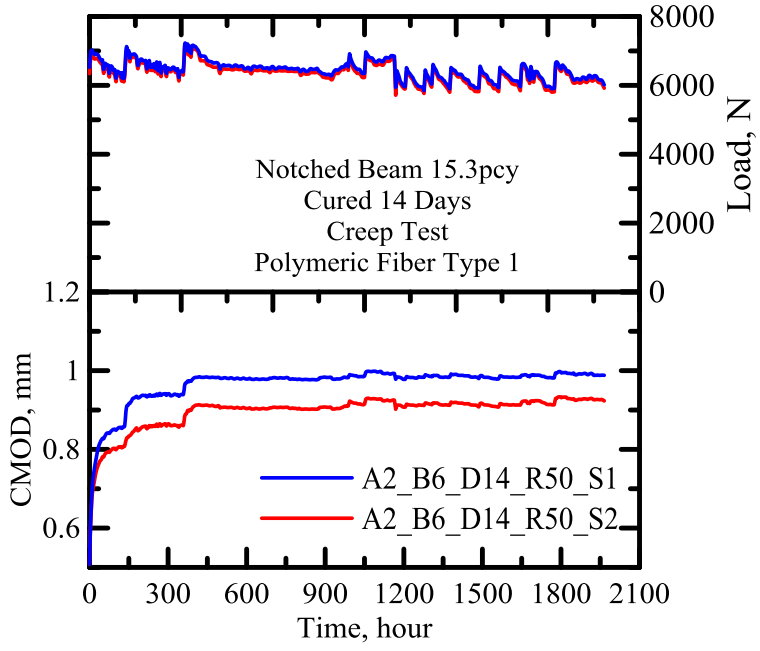

(b)

Figure 25: Responses for Specimen 1 & 2 for Polymeric Fiber Type 1 Fiber, (a) Load CMOD Curves for both Fracture and Creep Tests, (b) Load and CMOD vs Time Histories of Creep Test

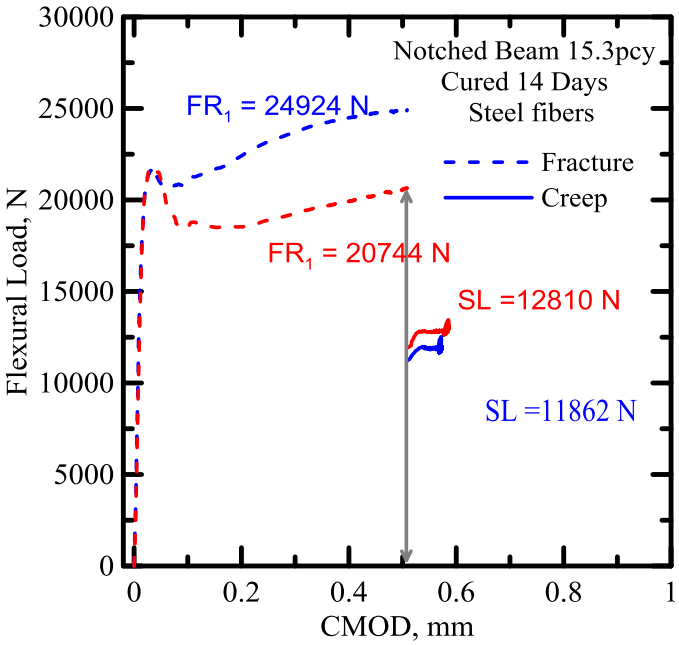

(a)

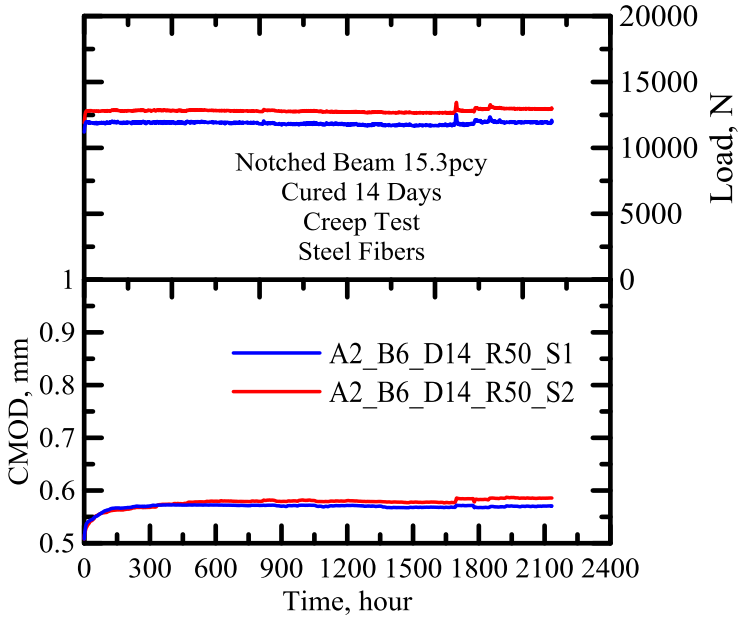

(b)

Figure 26: Responses for Specimen 1 & 2 for Steel Fibers Fiber, (a) Load CMOD Curves for both Fracture and Creep Tests, (b) Load and CMOD vs Time Histories of Creep Test

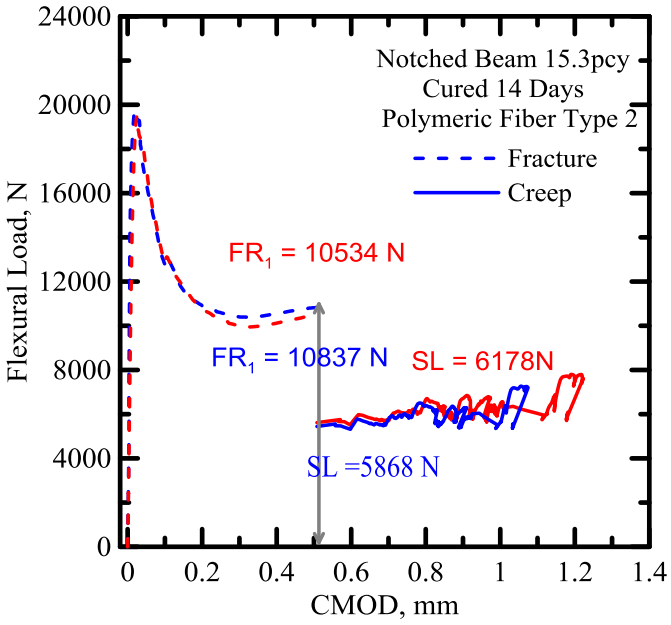

(a)

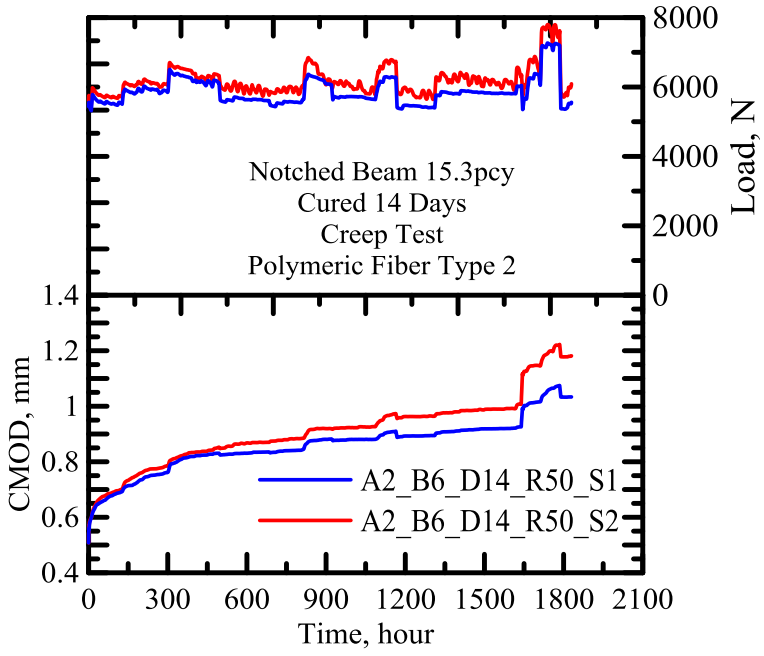

(b)

Figure 27: Responses for Specimen 1 & 2 for Polymeric Fiber Type 2 Fiber, (a) Load CMOD Curves for both Fracture and Creep Tests, (b) Load and CMOD vs Time Histories of Creep Test

Table 13: CMOD values of preliminary beam specimens after 75 days of creep (the final values of CMOD include the CMOD1 of 0.02 in.)

Fiber Type	S	Avg. Service	CMOD (mm)	CMOD (in)	Age (hours)	Flexural Failure	FR1
Polymeric Fiber Type 1	1	6435.06	0.4906	0.0193	2132.99	No	11813.4
Polymeric Fiber Type 1	2	6340.47	0.4255	0.0168	2132.99	No	12184.95
Polymeric Fiber Type 2	1	5856.06	0.5665	0.0223	1997.62	No	10837.34
Polymeric Fiber Type 2	2	6165.875	0.7142	0.0281	1997.62	No	10534.53
Steel Fibers	1	11862.67	0.0648	0.0026	2133.18	No	24924.29
Steel Fibers	2	12810.25	0.0792	0.0031	2133.18	No	20744.3

It was observed that polymeric fiber reinforced concrete experience larger creep deformations than steel fiber reinforced concrete [3]. Larger creep coefficients observed in cracked synthetic FRC mean greater creep deflections than comparable cracked steel FRC. Bernard [19] studied the creep of cracked FRC specimens based on ASTM C1550 [20]. Results indicated that high modulus synthetic macro fiber had creep behavior similar to steel fiber, whereas low modulus synthetic macro fiber experienced much higher creep.

3. Phenomenological and Rheological Models of Creep of Cracked FRC

3.1 Introduction

Extensive data generated from the experimental plan requires a procedure to develop a verification and validation the data. Curve fitting was carried out using different approaches to validate the experimental data. Curve Fitting is a process of constructing a curve or a mathematical expression such that it best fits the series of data points that show the varying creep coefficient values with respect to time. Two main approaches were adopted to get started with the curve fittings:

- Generate a creep coefficient curve for the experimental data.
- Fit the ACI and Reinhardt model to the experimental data.
- Generate a mathematical expression that curve fits the ACI model and the experimental data as well.

The latter part of the chapter also deals with the rheological viscoelastic models and their curve fits.

3.1.1 Experimental Data

The CMOD and force values for the creep tests were acquired at constant time intervals with the data acquisition system. To first plot the experimental data the creep coefficient curve was required. The Creep Coefficient values were generated using the following equation.

$$\varphi(t) = \frac{CMOD(t)}{CMOD\_initial} - 1$$

Thus, creep coefficient was defined as the ratio of the CMOD at each time interval with the initial CMOD. The same equation was used for calculating the creep coefficient by P. Pujadas [21].

The creep coefficients were calculated for the six specimens of Phase 2 which are, two beams with Polymeric Fiber Type 1 fiber with 7.5%, 10% and 15.3% fiber content each. The plots for the same were made with respect to time as given below.

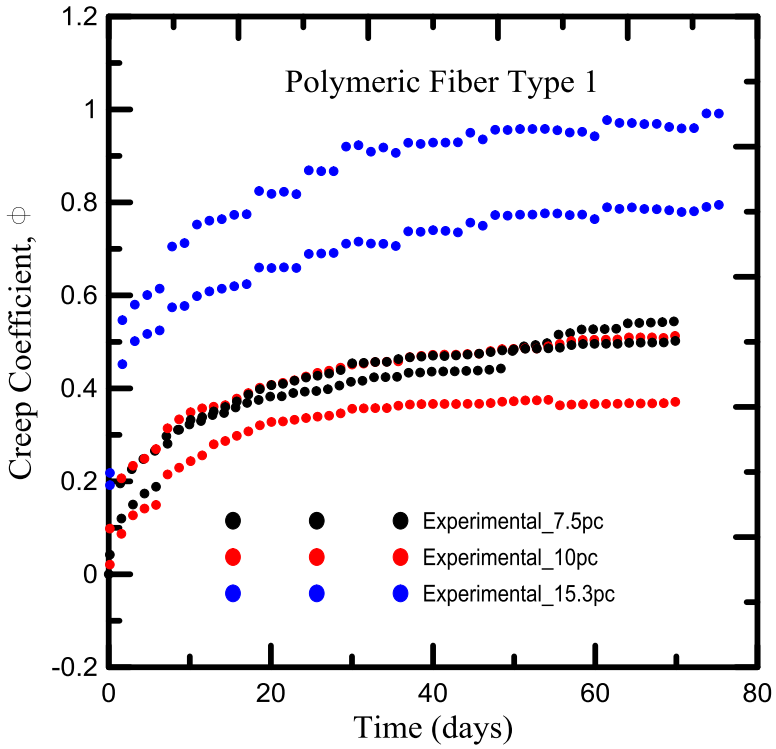

Figure 28: Creep Coefficient versus Time plot for the Phase 2 Experimental data with varying fiber content

3.2 Phenomenological Models

This section includes the curve fits for the creep coefficient plots generated using established models like the ACI 209-R 92 Model and the Reinhardt Model. The details and descriptions for each type are given below.

3.2.1 The ACI 209-R 92 Model

ACI has given a model that predicts the creep coefficient. The model given by ACI 209-R 92 had two main components that determine the asymptotic value and the time development of the creep. The parameter that was predicted by this model was the creep coefficient, φ which was given by the following equation.

$$\varphi(t,t_c) = \frac{(t-t_c)^{\psi}}{d+(t-t_c)^{\psi}} \cdot \varphi_u$$

φ_u is the ultimate creep coefficient which is defined as the ratio of the creep strain to the initial strain. As the experimental data does not have strains measured, the ultimate creep coefficient is considered as the ratio of the final CMOD value to the initial CMOD.

The term t signifies the total age of the specimen in days and t_c denotes the age of the specimen at which the creep load is applied. The terms ψ and d are given as shape and size constants which have an average value of 0.6 and 10 respectively by ACI. The parameters ψ and

d were adjusted to obtain a good curve fit of the experimental data to the ACI model. The curve fitting was carried out using the MATLAB curve fitting application. The following parameters were obtained for each type of specimen.

Table 14: Parameters obtained to fit the ACI 209-R 92 Model to the experimental data

Fiber Content	Parameter Ψ	Parameter d
Polymeric Fiber Type 1 7.5% Beam 1	0.3606	9.107
Polymeric Fiber Type 1 7.5% Beam 2	0.3384	10.1
Polymeric Fiber Type 1 10% Beam 1	0.3128	7.142
Polymeric Fiber Type 1 10% Beam 2	0.3821	9.81
Polymeric Fiber Type 1 15.3% Beam 1	0.2554	3.635
Polymeric Fiber Type 1 15.3% Beam 2	0.2863	3.299

It was observed that the values of both the parameters had a decreasing trend with an increase in the fiber content of the specimen and an increase in the sustained load on the specimen. The plot obtained after curve fitting the ACI model to the experimental data has been given below.

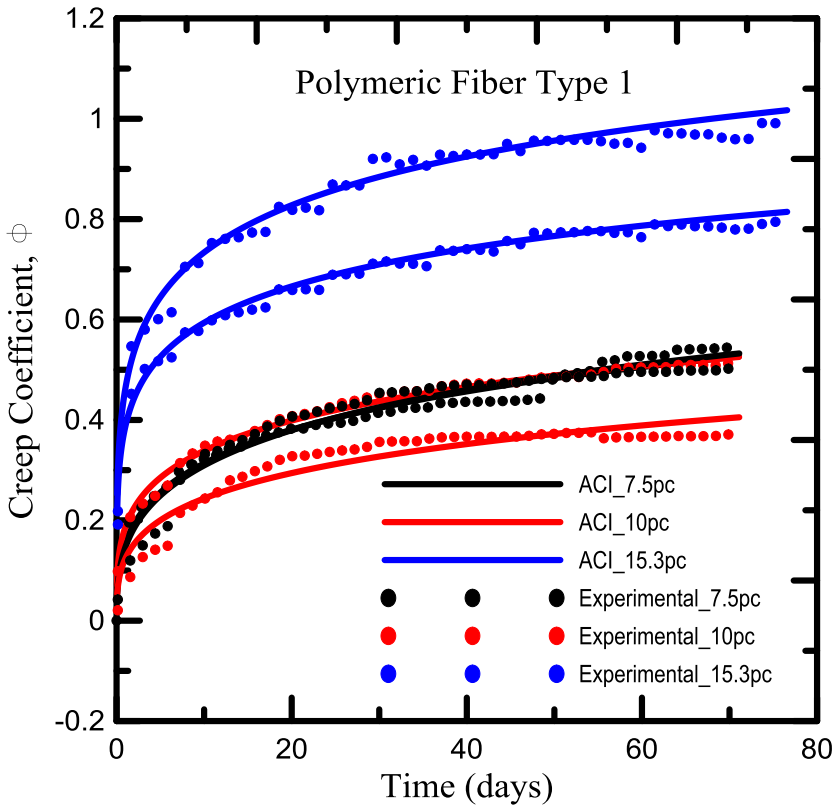

Figure 29: Creep Coefficient versus Time plot for the ACI 209-R 92 Model with the experimental data

3.2.2 Log Curve Fit for ACI 209-R 92 Model

A mathematical expression was used to fit the experimental data. After trial and error procedure, a log type of equation was used to generate curve fits for the experimental data. The equation for the curve fit has been given below:

$$y = f(x) = a\log(x) + b$$

In this equation, the parameter ‘y’ i.e. the creep coefficient which is a function of ‘x’. ‘x’ is time in days. With the curve fitting done, the plot obtained has been given below.

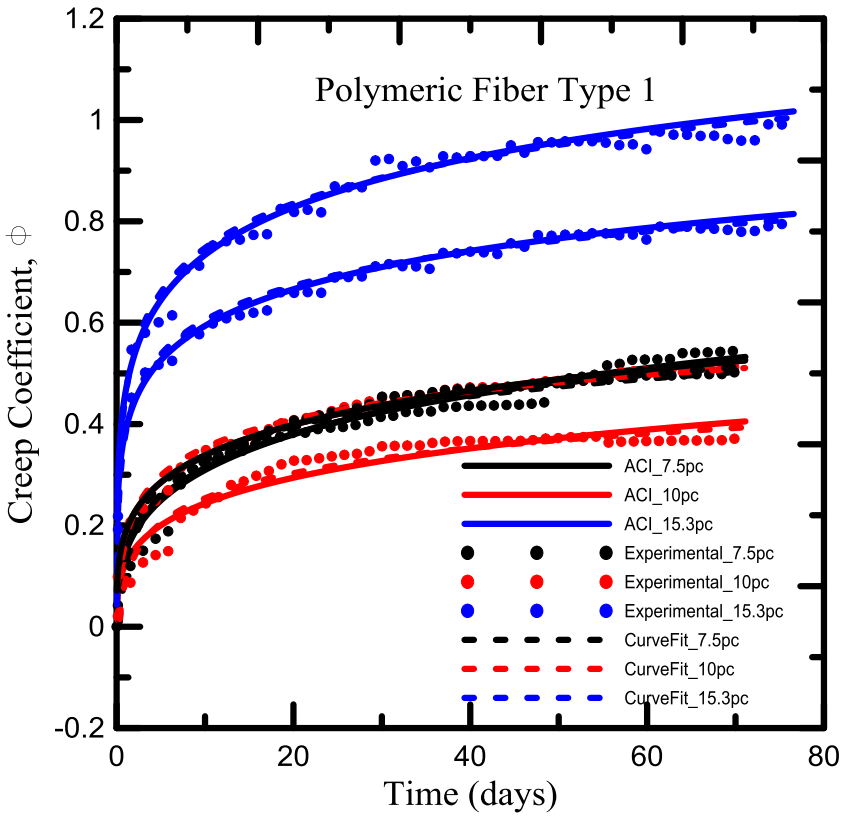

Figure 30: Creep Coefficient versus Time plot for the Curve Fit data using a Log Equation for the ACI 209-R 92 Model

The values obtained for the curve fitting of the log curve for the parameters ‘a’ and ‘b’ are given in table 15.

Table 15: Parameters obtained for the Log Curve Fit of the ACI 209-R 92 Model

Fiber Content	Parameter a	Parameter b
Polymeric Fiber Type 1 7.5% Beam 1	0.085	0.1414
Polymeric Fiber Type 1 7.5% Beam 2	0.7141	0.08899
Polymeric Fiber Type 1 10% Beam 1	0.08009	0.1691
Polymeric Fiber Type 1 10% Beam 2	0.09526	0.1076
Polymeric Fiber Type 1 15.3% Beam 1	0.09766	0.3802
Polymeric Fiber Type 1 15.3% Beam 2	0.1265	0.4561

3.2.3 The Eurocode-Reinhardt Curve Fit

Reinhardt [22] defined the creep coefficient of a structural element with an equation that was modified from the Eurocode 2 and the CEB-FIP MC90. In this model, the creep coefficient of a structural element at the time 't' that is loaded at a time 't_0' was calculated using the following equation:

$$\varphi(t,t_0) = \varphi_{RH}.\beta(f_{cm}).\beta(t_0).\beta_c(t,t_0)$$

Where the various terms can be explained as follows:

$$\varphi_{RH} = \left[1 + \frac{1 - RH/RH_0}{\sqrt{[3]0.1.h/h_0}}.\alpha_1\right].\alpha_2$$

Where,

$$\alpha_1 = \left(\frac{3.5 f_{cmo}}{f_{cm}} \right)^{0.7} \text{ and } \alpha_2 = \left(\frac{3.5 f_{cmo}}{f_{cm}} \right)^{0.2}$$

$$\beta(f_{cm}) = \frac{5.3}{\sqrt{f_{cm} / f_{cmo}}}$$

$$\beta(t_0) = \frac{1}{0.1 + (t_0 / t_1)^{0.2}}$$

$$\beta_c(t, t_0) = \left[\frac{(t - t_0) / t_1}{\beta_H + (t - t_0) / t_1} \right]^{0.3}$$

$$\beta_H = 150[1 + (1.2RH / RH_0)^{18}]h / h_0$$
$$+250.\alpha_3 \leq 1500.\alpha_3$$

Where the value of α_3 was given as the following,

$$\alpha_3 = \left(\frac{3.5 f_{cmo}}{f_{cm}} \right)^{0.5}$$

The f_{cm} parameter i.e. the mean compressive strength of the material at 28 days for the experimental specimen was used. The values are given below in Table 16.

Table 16: Mean Compressive Strength of the material of the Specimen tested in Phase 2

Fiber Content	f_{cm} , psi	f_{cm}, MPa
Polymeric Fiber Type 1 7.5% Beam 1	4468	30.80
Polymeric Fiber Type 1 7.5% Beam 2	4799	33.09
Polymeric Fiber Type 1 10% Beam 1	4144	28.57
Polymeric Fiber Type 1 10% Beam 2	4702	32.52
Polymeric Fiber Type 1 15.3% Beam 1	7562	52.14
Polymeric Fiber Type 1 15.3% Beam 2	6876	47.40

The plot obtained after using the above given model has been given in Figure 31. A good prediction for the lower fiber content samples was observed, however, it became inefficient for the higher fiber content samples.

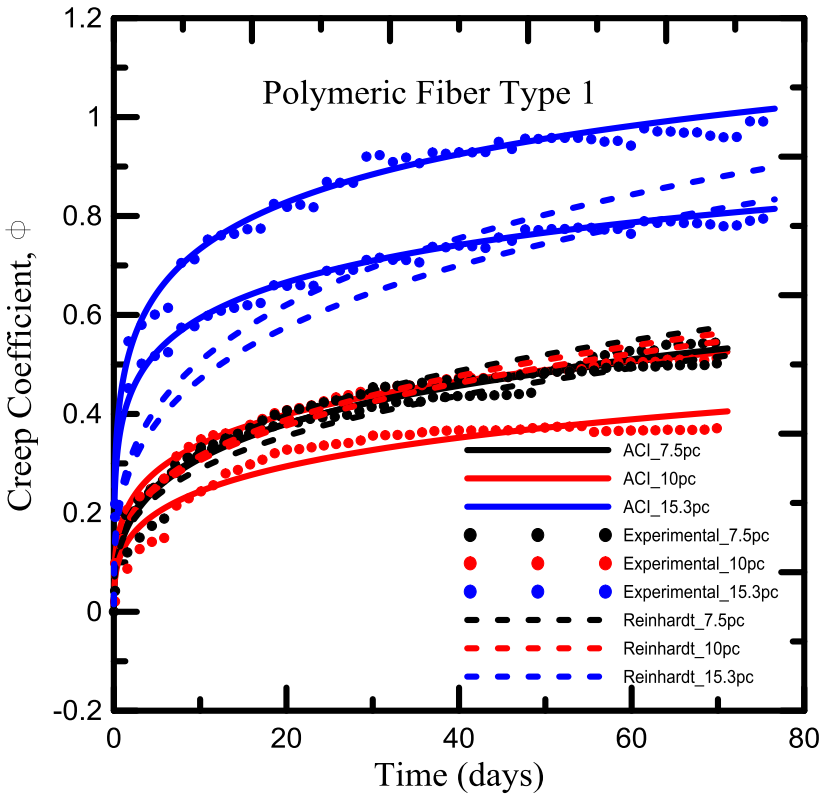

Figure 31: Creep Coefficient versus Time plot for the ACI 209-R 92 Model and the CEB-FIP Model

3.3 Rheological Models

The study by Rossi et al [23] concerned the relationship between compressive, tensile and flexural creep behaviors related to the same concrete. Various experimental tests along with a numerical simulation were performed in the scope of this plan. It is known that creep mainly falls into two categories:

- Basic Creep
- Shrinkage Creep

In this paper, the studies were limited to Basic Creep. To achieve the same, the drying effect of the concrete was controlled by gluing a double thickness of self-adhesive aluminum tape all over the specimen. After carrying out the compressive, tensile and bending creep testing and generating a data set, the specific creep curves were plotted for the same batch of concrete. Specific Creep curves are basically strain versus time per unit of applied stress.

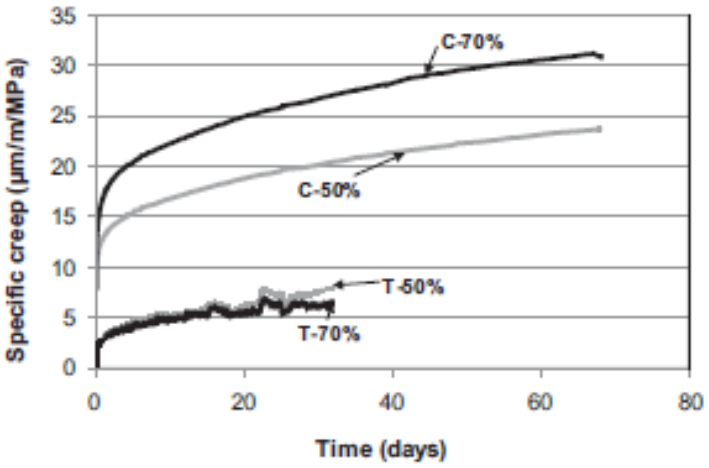

Figure 32: Specific Creep versus Time plot as given by Rossi et al [23]

These experimental Specific Creep Results were fitted by using mathematical functions of the form given below.

$$J_k(t) = \sum_{i=1,n_k} J_i \left(1 - \exp\left(\frac{t}{\theta_i}\right)\right)$$

Which corresponded to n_k (k = c in compression and k = t in tension) cells of a Kelvin-Voight chain with the Elastic Modulus and the viscosities given by the following equations:

$$E_i = \frac{1}{J_i} \text{ and } \eta_i = \frac{\theta_i}{J_i}$$

And thus the specific creep was expressed as the following,

$$\frac{\varepsilon_k(t) - \varepsilon_k^{el}}{\sigma_k} = \sum_{i=1,n_k} E_i \left(1 - \exp\left(\frac{t}{\eta_i / E_i}\right)\right)$$

Figure 33 shows the graph which expresses the Specific Creep versus Time plot for the experimental data. Specific Creep was defined as the ratio of creep coefficient and the stress on the area of the specimen. The Rheological Kelvin Voigt Chain used by Rossi et al [24] has been given in figure 33.

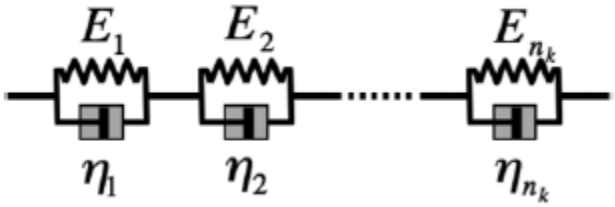

Figure 33: Rheological Kelvin Voigt Chain used by Rossi Et al [23]

A trial and error approach was adopted to fit a variety of viscoelastic models to the experimental data and to recognize the best model to portray the behavior of the material.

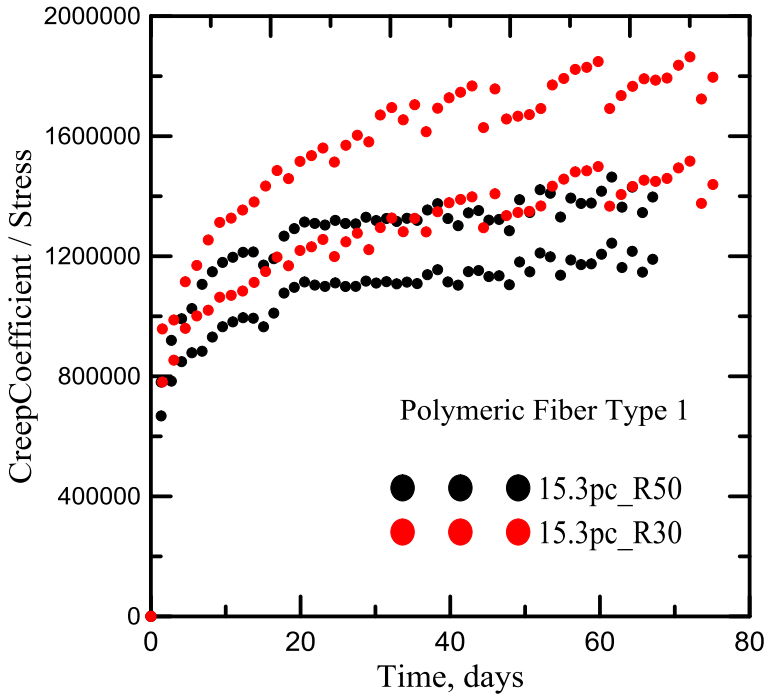

Figure 34: Specific Creep versus Time plot for the Experimental Data

3.3.1 Creep Compliance

The Creep Compliance curve for the experimental data was developed by defining compliance as the ratio of the increase in the Crack Mouth Opening Displacement (CMOD) value to the initial CMOD to the stress acting on the specimen. The CMOD values for the experiments were acquired at an interval of 6 seconds by a Data Acquisition System. Thus Creep Compliance was expressed as:

$$Creep\ Compliance(t) = \frac{CMOD(t)\ -\ CMOD\_initial}{Stress}$$

The creep compliance curves obtained for the specimens with the type 1 and type 2 polymeric fibers and steel fibers with respect to time are given in figure 35.

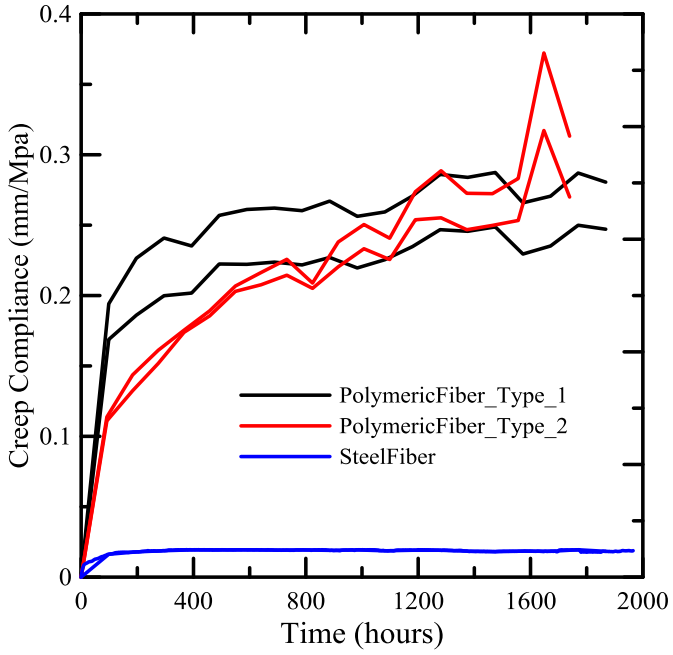

Figure 35: Phase 3 Experimental Creep Compliance versus Time Plot

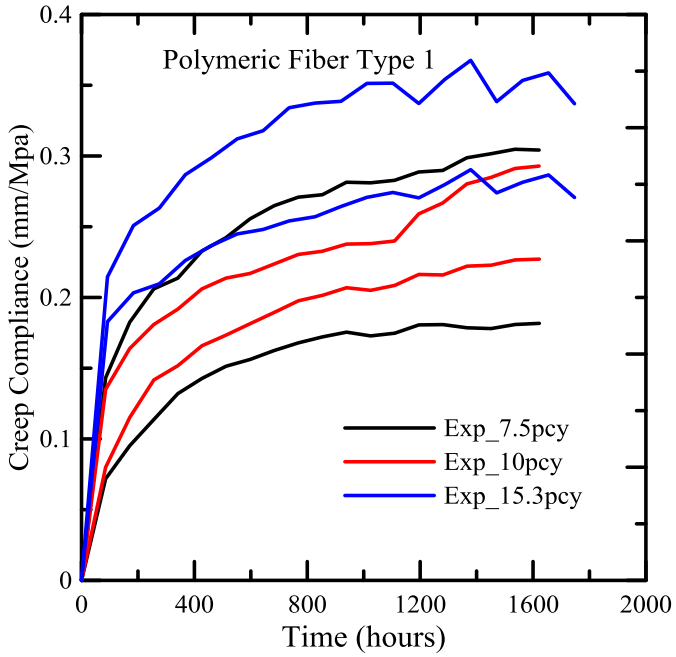

Figure 36: Phase 2 Experimental Creep Compliance versus Time Plot

It was observed that the Creep Compliance for the steel beams had a very low response as the CMOD values were very less and the stress applied to the beams was very high. Whereas, there was a vast difference in the response of the Polymeric Fibers. In order to understand these responses better, the experimental data was fit to various Viscoelastic models and corresponding material parameters were obtained.

3.3.2 Rheological Viscoelastic Models

A detailed study on various rheological viscoelastic models was carried out in order to apply a rheological viscoelastic model to the experimental study. The term viscoelastic defines a material that portrays both viscous and elastic behavior. The model of viscoelasticity can be

generated by combining the linear elastic spring and the linear viscous dashpot.

The constitutive equation for a material which behaves like a linear elastic spring is given by $\varepsilon = \frac{1}{E} * \sigma$. A dash-pot responds with a strain rate proportional to stress given as $\dot{\varepsilon} = \frac{1}{\eta} * \sigma$. In a dashpot, any strain built up due to stress is permanent even after the removal of the applied stress. Thus the relationship between the stress and strain during the creep-test and the Creep Recovery Response of a dashpot may be expressed in the given form:

$$\varepsilon(t) = \sigma_0 * J(t); where\ J(t) = \frac{t}{\eta}$$

Using these very simple material properties, the basic viscoelastic models can be generated which are:

- Maxwell Model
- Kelvin-Voight Model

Hybrid models can be generated by considering combinations of the basic models as given below:

- Three Element Hybrid Model
- Four Element Hybrid Model

- Five Element Hybrid Model

3.3.2.1 MAXWELL MODEL

The Maxwell model is developed by connecting a spring and a dash-pot element in series as given below.

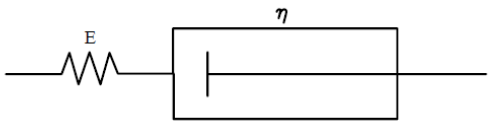

Figure 37: Maxwell Model

The equilibrium requires that the stress should remain constant throughout the spring and the dashpot. Thus the strain was given as the summation of strain 1 in the spring (ε_1) and the strain 2 in the dashpot (ε_2). The basic equilibrium equations used to derive the model as follows:

$$\varepsilon_1 = \frac{1}{E}\sigma \ , \ \dot{\varepsilon}_2 = \frac{1}{\eta}\sigma \ \text{ and } \ \varepsilon = \varepsilon_1 + \varepsilon_2$$

Now, taking the derivative of strain with respect to time we obtained the following:

$$\frac{d\varepsilon_{total}}{dt} = \frac{d\varepsilon_D}{dt} + \frac{d\varepsilon_s}{dt} = \frac{\sigma}{\eta} + \frac{1}{E}\frac{d\sigma}{dt}$$

Thus, the Maxwell Model is expressed as,

$$\frac{1}{E}\frac{d\sigma}{dt}+\frac{\sigma}{\eta}=\frac{d\varepsilon}{dt}$$

Considering the initial stress as σ_0, the creep compliance equation J(t) was derived from the Maxwell model as the following:

$$\varepsilon(t)=\sigma_0 J(t)\text{, where, } J(t)=\frac{t}{\eta}+\frac{1}{E}$$

3.3.2.2 KELVIN VOIGT MODEL

The Kelvin – Voigt model is another basic two element model. A figure of the same is given below in figure 38.

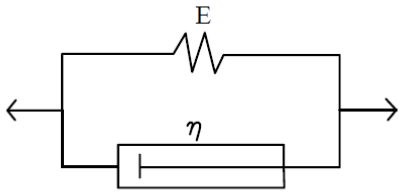

Figure 38: Kelvin Voigt Model

The Kelvin – Voight Model consists of a spring element and a dash-pot element connected in parallel to each other. Assumption is made that there is no bending in this model thus the train experienced is the same in both the spring and the dashpot element. Thus the boundary conditions are given as the following:

$$\varepsilon = \frac{1}{E}\sigma_1 \ , \ \dot{\varepsilon} = \frac{1}{\eta}\sigma_2 \ \text{ and } \ \sigma = \sigma_1 + \sigma_2$$

Where σ_1 is the stress in the spring element and σ_2 is the stress in the dashpot element. From the above given equations it was concluded that the stress, strain and their rate of change with respect to time 't' were governed by the following equation:

$$\sigma(t) = E\varepsilon(t) + \eta \frac{d\varepsilon(t)}{dt}$$

This equation could also be expressed as the following:

$$\sigma = E\varepsilon + \eta \dot{\varepsilon}$$

The Creep Recovery Response in a Kelvin Voigt Model is a lot different because of the parallel attachment of elements. When a stress σ_0 acts on a Kelvin Model, the spring with its natural tendency to stretch is held back by the dash-pot. Thus, the creep curve initially starts with a slope of σ_0/η which is the influence of the dashpot. As time progresses, stress from the dashpot is transferred to the spring and thus the slope changes to σ_2/η where σ_2 is the stress in the dashpot. When all the stress is transferred to the spring, the maximum strain then becomes σ_1/E. Thus, we obtain that,

$$\varepsilon(t) = \frac{\sigma_0}{E}(1 - e^{-(E/\eta)t})$$

Thus, the Creep Compliance function for the Kelvin Voigt Model is defined as,

$$J(t) = \frac{1}{E}(1 - e^{-t/t_r}) \text{ , where } t_r = \frac{\eta}{E}$$

The following plot was obtained for the creep compliance of specimen with respect to time.

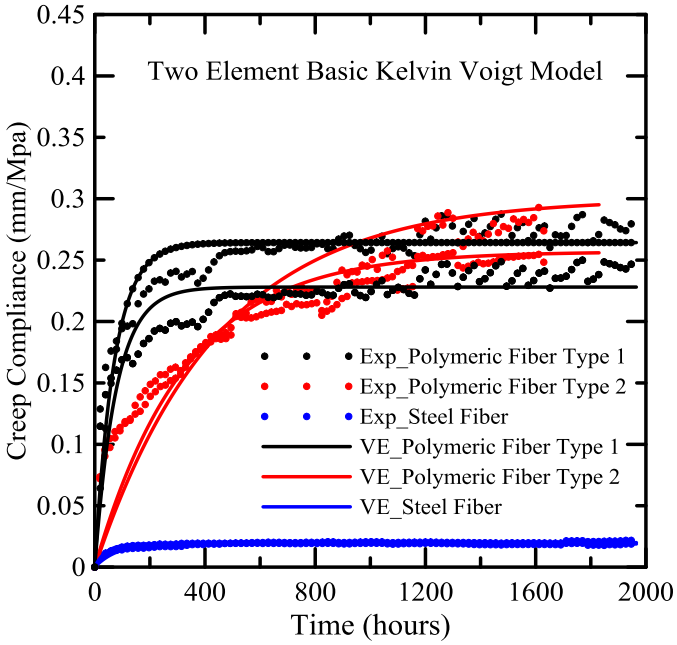

Figure 39: Phase 3 Two Element Model Creep Compliance versus Time

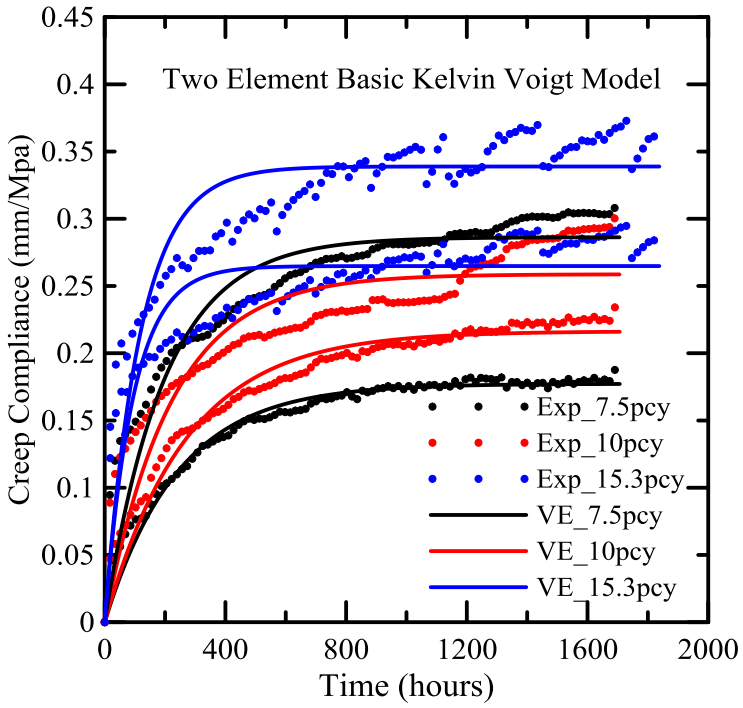

Figure 40: Phase 2 Two Element Model Creep Compliance versus Time

The parameters involved in plotting the Viscoelastic Model curves are given below for all specimen type:

Table 17: Two Element Viscoelastic Model Parameters for Phase 3

Specimen Type	Specimen number	E (MPa)	η
Macro Fiber Type 1	1	3.874	267.3
	2	4.385	340.6
Steel Fiber	1	53	2073
	2	50.09	4215
Macro Fiber Type 2	2	3.892	1278
	3	3.332	1492

Table 18: Two Element Viscoelastic Model Parameters for Phase 2

Specimen Type	Specimen number	E (MPa)	η
7.5 pc	1	3.865	850
	2	4.622	1253
10 pc	1	3.493	692.9
	2	5.64	1366
15.3 pc	2	3.776	356.8
	3	2.951	346.7

3.3.2.3 THREE ELEMENT HYBRID MODEL

A combination of one spring unit and one Kelvin Voigt unit was adopted to make the three-element hybrid model. A line diagram of the same has been expressed below:

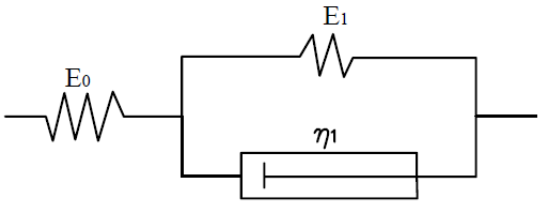

Figure 41: Three Element Hybrid Viscoelastic Model

The equation given below shows the compliance for a three-element model and the creep compliance curves obtained using this equation are plotted in figure 42.

$$J(t) = \frac{1}{E_0} + \frac{1}{E_1}(1 - e^{-tE_1/\eta_1})$$

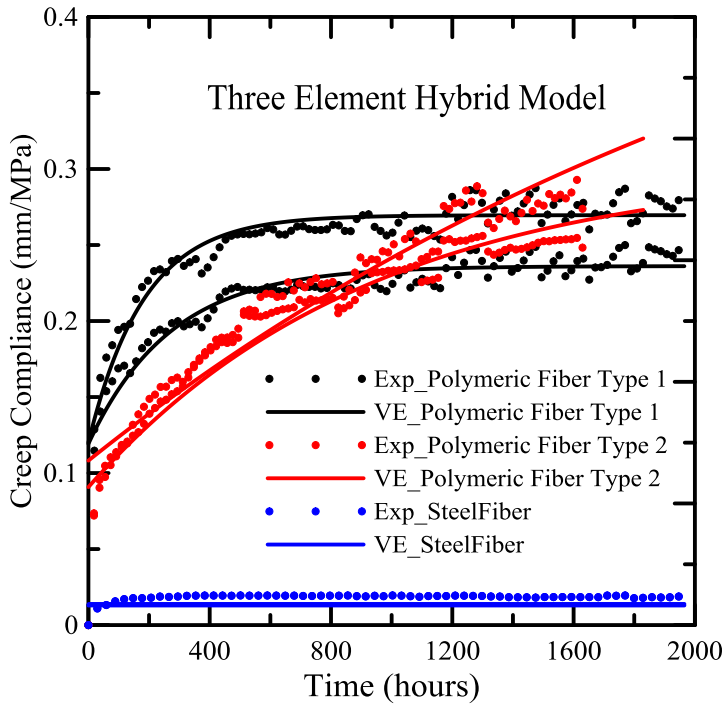

Figure 42: Phase 3 Three Element Model Creep Compliance versus Time

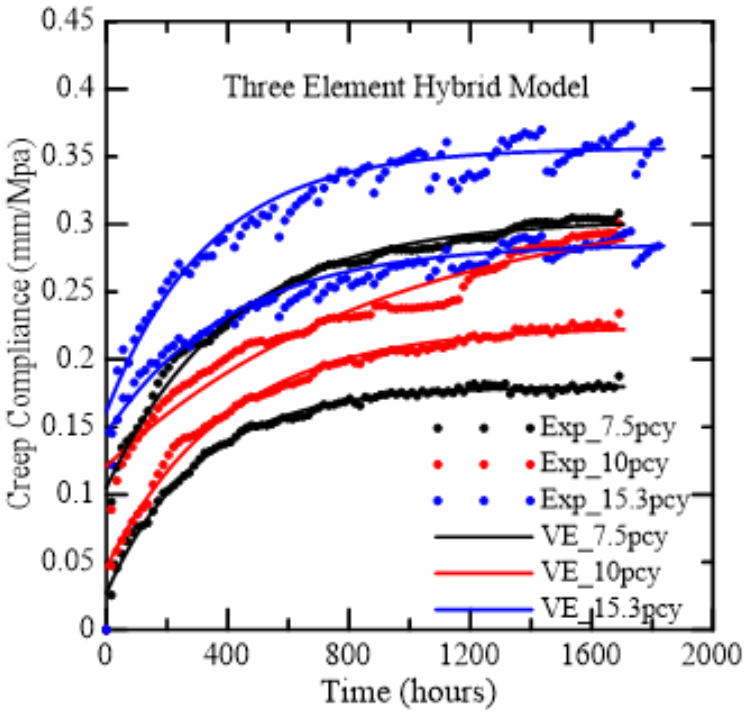

Figure 43: Phase 2 Three Element Model Creep Compliance versus Time

Table 19: Three Element Model Parameters for Phase 3

Specimen Type	Specimen number	E_0 (MPa)	E_1 (MPa)	η_1
Polymeric Fiber Type 1	1	8.325	6.689	1229
	2	8.389	8.551	2316
Steel	1	73.1	4549	190.6
	2	78.01	13690	134.1
Polymeric Fiber Type 2	2	11.02	4.716	4391
	3	9.244	2.332	6261

Table 20: Three Element Model Parameters for Phase 2

Specimen Type	Specimen number	E_0 (MPa)	E_1 (MPa)	η_1
7.5 pc	1	8.263	5.023	4681
	2	21.71	5.606	2213
10 pc	1	9.517	5.051	2084
	2	36.79	6.535	1984
15.3 pc	2	6.875	7.143	2961
	3	6.2	5.123	1726

3.3.2.4 FOUR ELEMENT HYBRID MODEL

The second hybrid model considered had two Kelvin Voigt models connected in series. A schematic of the four-element model is given below:

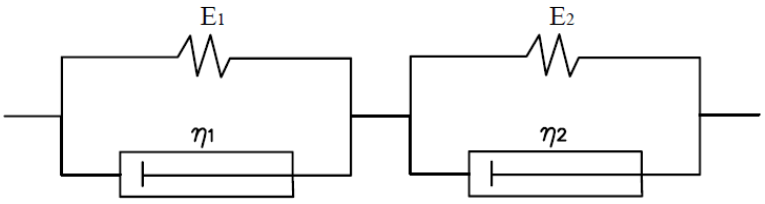

Figure 44: Four Element Hybrid Model

The compliance equation thus had 4 material parameters which were E_1, E_2, η_1 and η_2.

$$J(t) = \frac{1}{E_1}(1 - e^{-tE_1/\eta_1}) + \frac{1}{E_2}(1 - e^{-tE_2/\eta_2})$$

The creep compliance curves for the experimental data generated obtained by using the above given equation are given below.

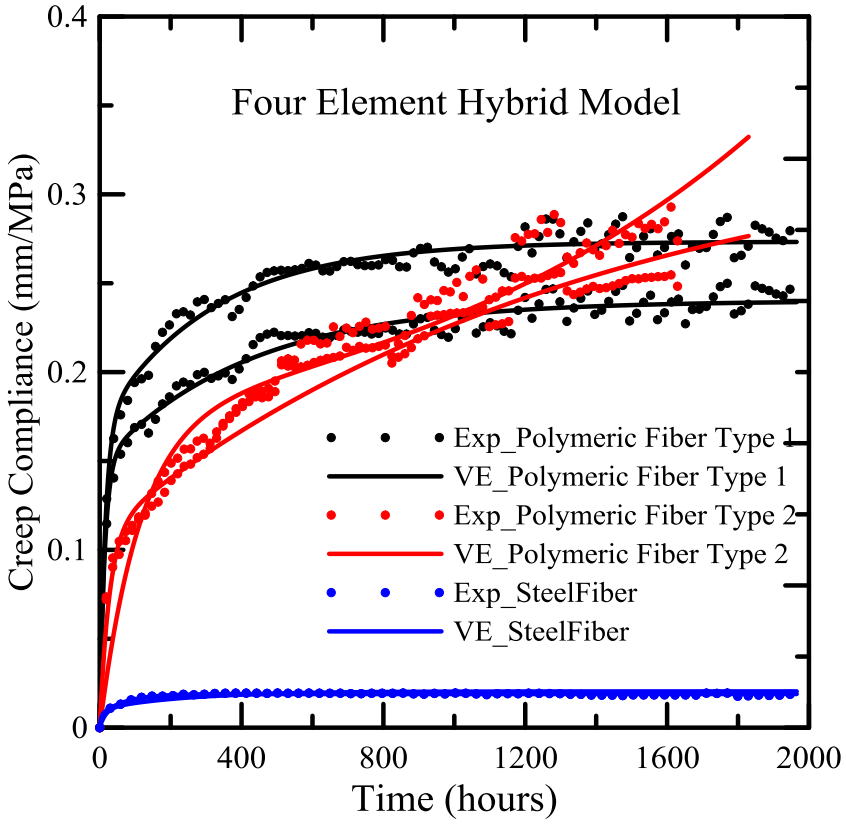

Figure 45: Phase 3 Four Element Model Creep Compliance versus Time

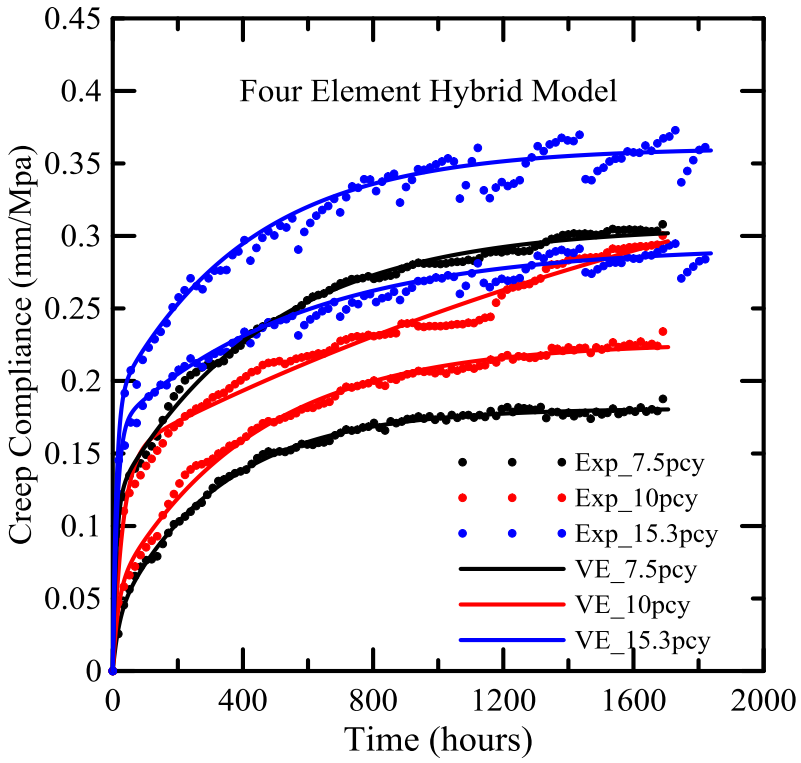

Figure 46: Phase 2 Four Element Model Creep Compliance versus Time

Table 21: Four Element Model Parameter for Phase 3

Specimen Type	Specimen number	E_1 (MPa)	η_1	E_2 (MPa)	η_2
Polymeric Fiber Type 1	1	9.683	3029	5.878	92.04
	2	10.94	4519	6.724	93.41
Steel Fiber	1	81.23	5605	150.9	486.3
	2	101.3	24260	94.85	1557
Polymeric Fiber Type 2	2	4.418	6041	9.126	247
	3	-26	29450	5.64	650.3

Table 22: Four Element Model Parameter for Phase 2

Specimen Type	Specimen number	E_1 (MPa)	η_1	E_2 (MPa)	η_2
7.5 pcy	1	3.361	8420	6.693	201.3
	2	5.851	2526	17.95	296.1
10 pcy	1	8.429	89.25	5.317	2479
	2	6.874	2245	28.03	524.7
15.3 pcy	2	5.961	78.2	7.988	4551
	3	5.389	58.47	5.702	2345

3.3.2.5 FIVE ELEMENT HYBRID MODEL

As discussed by Zhu et al [25], a hybrid five element Viscoelastic model can be used to predict the compliance of asphalt mastic beams in flexure. The applicability of this model to the experimental data was studied by simulating the data using this model. The viscoelastic model used was a combination of two Kelvin Voigt elements and a spring element all attached in series. The line diagram and the equation for the viscoelastic model are as given below:

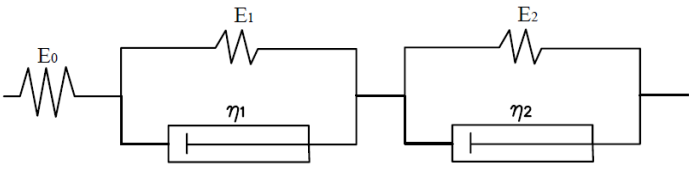

Figure 47: Five Element Hybrid Viscoelastic Model

$$J(t) = \frac{1}{E_0} + \frac{1}{E_1}(1 - e^{-tE_1/\eta_1}) + \frac{1}{E_2}(1 - e^{-tE_2/\eta_2})$$

Thus, the fit of this function obtained for the experimental data was as follows.

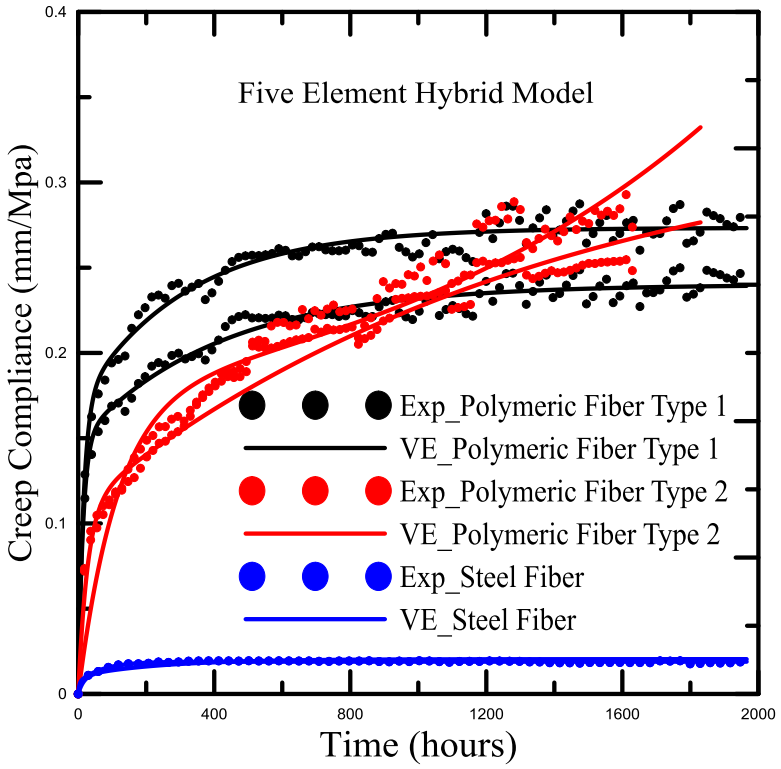

Figure 48: Phase 3 Five Element Model Creep Compliance versus Time

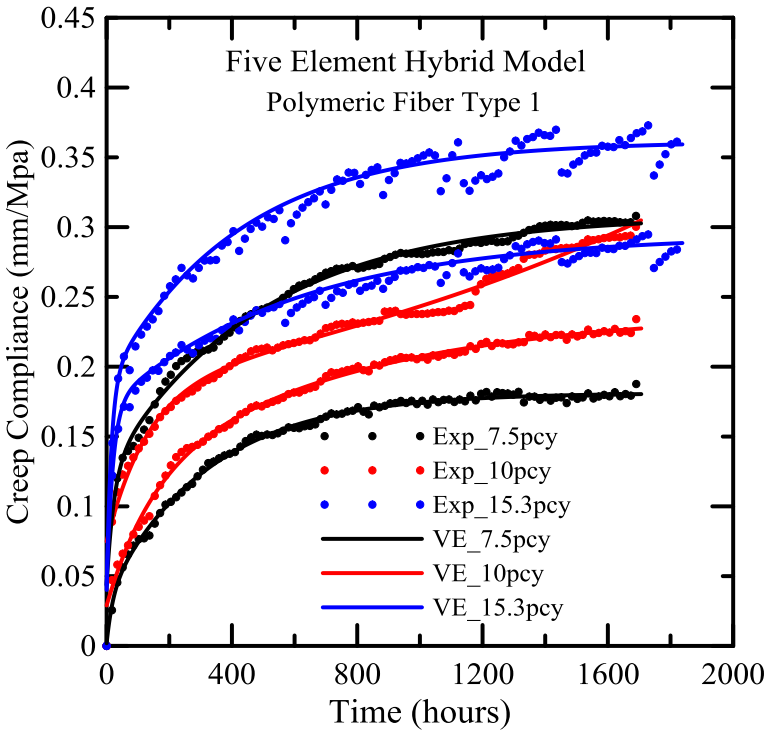

Figure 49: Phase 2 Five Element Model Creep Compliance versus Time

Observation was made that the nature fit of the compliance model got better with increased number of elements in the compliance equation. The values of the material parameters obtained after carrying out the compliance curve fits were as follows:

Table 23: Five Element Model Parameter for Phase 3

Specimen Type	Specimen number	E_1 (MPa)	E_2 (MPa)	η_1	E_3 (MPa)	η_2
Polymeric Fiber Type 1	1	30.78	10.51	3669	6.822	158.7
	2	33.14	8.147	161	11.37	5027
Steel Fiber	1	553.7	405.2	3.589	68.34	3766
	2	562.3	495.4	0.0154	61.6	6776

Polymeric Fiber Type 2	2	14.43	5.888	2476	-6899	2188000
	3	13.33	5.25	2663	-9781	2755000

Table 24: Five Element Model Parameter for Phase 2

Specimen Type	Specimen number	E_1 (MPa)	E_2 (MPa)	η_1	E_3 (MPa)	η_2
7.5 pcy	1	13.36	8.811	1168	-13.31	24250
	2	34.51	11.69	1664	7.966	5923
10 pcy	1	22.8	5.452	2691	12.32	289
	2	524.2	29.52	583.6	6.878	2248
15.3 pcy	2	23.2	8.126	4904	7.795	154.6
	3	24.95	5.777	2431	6.744	100.2

3.3.2.6 CONCLUSION FOR VISCOELASTIC MODEL

Thus, it was concluded that, the more elements a model has, the more accurate it was in describing the response of real materials. Although the determination of more number of parameters becomes a tedious task, it increases the accuracy of the prediction of the compliance.

In the study it was observed that the prediction of compliance was best done by the model which has 5 different material parameters. The second closest was the type 1 hybrid model where the compliance was predicted by connecting two Kelvin Voigt Models in Series. It was noticed that the prediction for the Type 2 hybrid model was not too accurate

especially at the beginning of the plot. This behavior was explained because of the presence of the spring along with the Kelvin Voigt unit which tends to deform as soon as the stress is applied and again goes back to its original position once it is released, showing more of an elastic behavior. This contradicted the behavior of a concrete as a material, as concrete does not tend to display an elastic behavior on unloading.

4. Creep Prediction Model

4.1 Introduction

For various real life problems, analytical equations can be used for selection of variables using a design automation procedure. For tackling the same, analytical solutions to address the flexural creep behavior of plain FRC have been developed. Moment-curvature relationships can be generated using closed form equations. The notations used are as follows:

b = beam width

d = beam depth

E = tensile modulus

E_c = compressive modulus

E_{cr} = post crack tensile modulus

F = force component

f = stress at vertex in stress diagram

h = height of each zone in stress diagram

k = neutral axis depth ratio

L = clear span

M_{cr} = moment at first cracking

M_i' = normalized moment

P = total load applied to three point bending beam specimen

p = depth of neutral axis at the time of first cracking

y = moment arm from neutral axis to center of each force component

α = normalized transition strain

β = normalized tensile strain at bottom fiber

β_{tu} = normalized ultimate tensile strain

ε_c = compressive strain

ε_{cr} = first cracking tensile strain

ε_{ctop} = compressive strain at top fiber

ε_{cu} = ultimate compressive strain

ε_{cy} = compressive yield strain

ε_t = tensile strain

ε_{tbot} = tensile strain at bottom fiber

ε_{tu} = ultimate tensile strain

γ = normalized concrete compressive modulus

λ = normalized compressive strain

λ_{cu} = normalized ultimate compressive strain

σ_c = compressive stress

σ_{cr} = cracking tensile strength

σ_{cst} = constant tensile stress at the end of the tension model

σ_{cy} = compressive yield stress

σ_t = tensile stress

ω = normalized compressive yield strain

4.2 Uniaxial Tensile and Compressive Constitutive Model

As given in the study by Soranakom and Mobasher [26], Figure 50 represents a constitutive model for fiber reinforced concrete under static loading. As shown in Figure 50(a), the linear portion of an elastic-perfectly-plastic compressive stress-strain response terminates at yield point (ε_{cy}, σ_{cy}) and remains constant at compressive yield stress σ_{cy} until the ultimate compressive strain ε_{cr}. The tension model in part b has been described by a trilinear response. The elastic range has been defined by E in the tension model and later Ecr is used for defining the softening or the hardening zones. The third region was defined by σ_{cst} in the post crack region. For sustained loads and creep the value of μ changes at every step and thus we can plot the experimental response accordingly. A linear stress response was obtained in the third zone. ε_{cr} is the main strain measure used to define

the first cracking strain. The transition strain and the first cracking strain value are considered to be the same in this case as there is no transition strain considered. The tensile response terminates at the ultimate tensile strain level of ε_{tu}. The stress strain relationship for compression are expressed as:

$\sigma_c(\varepsilon_c) = E_c\varepsilon_c$ $\quad 0 \leq \varepsilon_c \leq \varepsilon_{cy}$

$\sigma_c(\varepsilon_c) = E_c\varepsilon_{cy}$ $\quad \varepsilon_{cy} \leq \varepsilon_c \leq \varepsilon_{cu}$

$\sigma_c(\varepsilon_c) = 0$ $\quad \varepsilon_c > \varepsilon_{cu}$

Whereas the stress strain relationship for tension are expressed as the following:

$\sigma_t(\varepsilon_t) = E\varepsilon_t$ $\quad 0 \leq \varepsilon_t \leq \varepsilon_{cr}$

$\sigma_t(\varepsilon_t) = E\varepsilon_{cr}$ $\quad \varepsilon_t = \varepsilon_{cr}$

$\sigma_t(\varepsilon_t) = \mu E\varepsilon_{cr}$ $\quad \varepsilon_{cr} \leq \varepsilon_t \leq \varepsilon_{tu}$

$\sigma_t(\varepsilon_t) = 0$ $\quad \varepsilon_t \geq \varepsilon_{cr}$

Where, σc , σt , εc and εt, are compressive and tensile stresses and strains respectively. In order to derive the closed form solutions for moment-curvature response, the material parameters given in Figure 49 are defined as a combination of two intrinsic material parameters that is the first cracking tensile strain ε_{cr} and the tensile modulus E in addition to the following normalized parameters with respect to E and ε_{cr} as shown below:

$$\omega = \frac{\varepsilon_{cy}}{\varepsilon_{cr}} \; ; \; \alpha = \frac{\varepsilon_{trn}}{\varepsilon_{cr}} \; ; \; \beta_{tu} = \frac{\varepsilon_{tu}}{\varepsilon_{cr}} \; ; \; \lambda_{tu} = \frac{\varepsilon_{tu}}{\varepsilon_{cr}}$$

$$\gamma = \frac{E_c}{E} \; ; \; \mu = \frac{\sigma_{cst}}{E\varepsilon_{cr}}$$

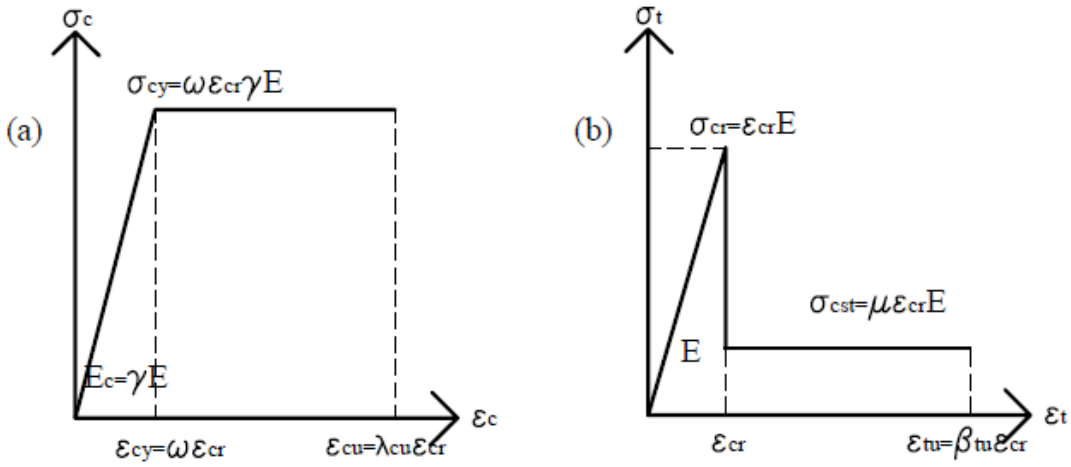

Figure 50: Material model for homogenized fiber reinforced concrete (a) compression model and (b) tension model

The normalized tensile strain at the bottom fiber β and the normalized compressive strain at the top fiber λ are defined as the following:

$$\beta = \frac{\varepsilon_{tbot}}{\varepsilon_{cr}} \; ; \; \lambda = \frac{\varepsilon_{ctop}}{\varepsilon_{cr}}$$

They are linearly related through the normalized neutral axis parameter k.

$$\frac{\lambda\varepsilon_{cr}}{kd} = \frac{\beta\varepsilon_{cr}}{d-kd} \quad \text{,or } \lambda = \frac{k}{1-k}\beta$$

Substitution of all the normalized parameters results in the following stress strain models.

The compressive stress strain model can be obtained using the following:

$$\frac{\sigma_c(\lambda)}{E\varepsilon_{cr}} = \gamma\lambda \qquad 0 \leq \lambda \leq \omega$$

$$\frac{\sigma_c(\lambda)}{E\varepsilon_{cr}} = \gamma\omega \qquad \omega \leq \lambda \leq \lambda_{cu}$$

$$\frac{\sigma_c(\lambda)}{E\varepsilon_{cr}} = 0 \qquad \lambda_{cu} < \lambda$$

The tensile stress strain model can be obtained using the following:

$$\frac{\sigma_t(\beta)}{E\varepsilon_{cr}} = \beta \qquad 0 \leq \beta \leq \alpha$$

$$\frac{\sigma_t(\beta)}{E\varepsilon_{cr}} = \mu \qquad \alpha \leq \beta \leq \beta_{tu}$$

$$\frac{\sigma_t(\beta)}{E\varepsilon_{cr}} = 0 \qquad \beta_{tu} \leq \beta$$

The stress strain diagrams obtained at distinct stages of normalized tensile strain at the bottom fiber (β) are given below.

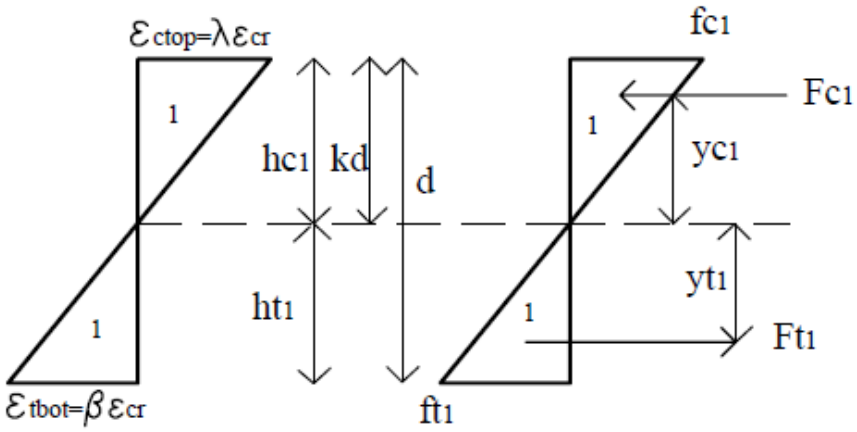

Figure 51: Stress Strain Diagram obtained for normalized tensile strain at the bottom fiber when $0 \leq \beta \leq \alpha$

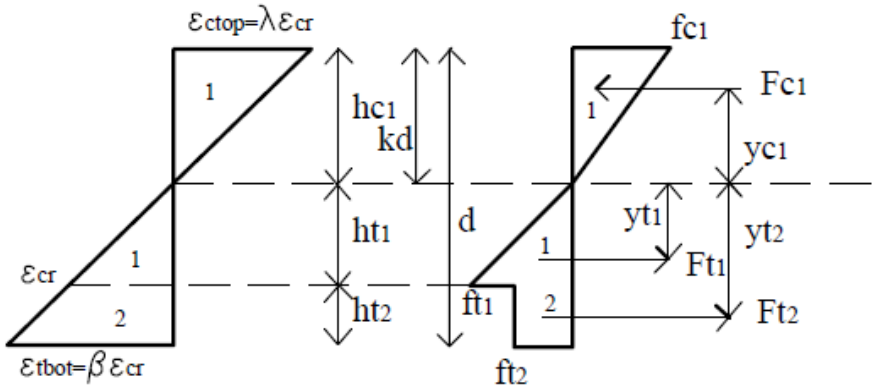

Figure 52: Stress Strain Diagram obtained for normalized tensile strain at the bottom fiber when $\alpha < \beta \leq \beta_{tu}$

4.3 Derivation of Moment Curvature Relationship

The Kirchhoff hypothesis of plane section remaining plane for flexural loading was applied for deriving the moment curvature diagram for

a rectangular cross section with a width b and depth d. By assuming linear strain distribution across the depth of the cross section and by ignoring the shear deformation, the stress-strain relationships in the above given figure were used to obtain the stress distribution across the cross section at two stages of imposed tensile strain: $1 \leq \beta \leq \alpha$, and $\alpha < \beta \leq \beta_{tu}$.

The neutral axis depth ratio was found by solving for the equilibrium of forces in the stress diagram. The moment capacity at the first cracking is calculated by taking tension and compressive forces around the neutral axis and the corresponding curvature was obtained by dividing the top compressive strain with the neutral axis depth. With an increase in strain after the first cracking, the creep response is considered and the moment is considered to stay constant along with a case of constant stresses in the compression and tension zone of the un-cracked region along with a varying residual stress in the cracked region.

Thus, by solving for the above given condition the value of the neutral axis depth ratio k and the residual tensile strength μ is calculated for every increasing strain value. The Moment M and the curvature φ were then normalized with their cracking moment Mcr and cracking curvature φcr values.

$$M_{cr} = \frac{1}{6} b d^2 E \varepsilon_{cr}$$

$$\phi_{cr} = \frac{2\varepsilon_{cr}}{d}$$

The expression for calculating the moment curvature and neutral axis for all stages of applied strain are given below. However, to develop a combined response for both the static and the creep tests on the specimen, the moment curvature response for the beam is stopped at the value of beta which is obtained by back-calculations when we reach the load FR_1 and a crack width of 0.02 inch is obtained.

Table 25: Neutral axis parameter k, normalized moment M' and normalized curvature for each stage of normalized tensile strain at bottom fiber

Stage	**k**	**M_i' and φ_i'**
1 **$0 < \beta \leq \alpha$**	$k_1 = \frac{-1+\sqrt{\gamma}}{-1+\gamma}$ for $\gamma < 1$ or $\gamma > 1$ $k_1 = \frac{1}{2}$ for $\gamma = 1$	$M_1' = -\frac{2\beta(1+(-1+\gamma)k^3+3k^2-3k)}{-1+k}$ $\phi_{cr} = -\frac{\beta}{2(-1+k)}$
2 **$\alpha < \beta \leq \beta_{tu}$**	$k_{21} = \frac{\beta^2\gamma + K21 + \sqrt{\gamma^2\beta^4 - \gamma\beta^2 K21}}{K21}$ $K21 = -2\mu\beta - 1 + 2\mu + \gamma\beta^2$	$M_{21} = -\frac{(-MM21+2\beta\gamma)k^3+3MM21k^2-3MM21k+MM21}{(-1+k)}$ $MM21 = \frac{2+3\mu\beta^2-3\mu}{\beta^2}$

Once the value of maximum moment is obtained for the FR_1 response, it is scaled down to the ratio of load reduction for unloading the beams from static loading and reloading it under creep loading. Thus, the new moment value obtained was be given by the following equation.

$$NewMoment = LoadingFactor * M\max$$

Where the reduction factor was the percentage at which the specimens were loaded in creep set up. Once the new moment value was obtained, the corresponding curvature was found considering unloading response to be linear. Thus, the new curvature was calculated using the following equation.

$$\phi_{new} = \phi_{old} - \phi_{diff}$$

$$\phi_{diff} = \frac{(1 - LoadingFactor)}{EI} * M \max$$

The Moment and curvature obtained defines the Moment-curvature relation of the specimen at the beginning of the creep loading. As curvature can be defined in terms of β and k, the strain diagram at the beginning of the creep loading was obtained by solving for the given three conditions.

- Force Equilibrium
- Constant Moment
- Curvature Relationship

Simultaneously solving for the values of β, k and μ helps us in generating the strain response. These form the initial values in the creep type response of the specimen material. To solve for the changing values of k and μ with an increasing β value, the value of moment was considered to be constant and the force equilibrium equation was brought in terms of μ. Thus substituting the equation of μ, solution for k was obtained for a constant moment. The set of equations obtained for the same are given below.

From the force equilibrium equation,

$$\mu = -\frac{k - kp + \beta\beta_1\gamma kp - 1 + p}{2kp + 2\beta k - 2\beta kp - 2k - 2\beta + 2\beta p + 2 - 2p}$$

Now substituting the value of μ and simplifying the equation, the equation for zero moment was derived as,

$$M_{21} = ak^2 + bk + c$$

Where, $a = -(\beta^2\beta_1\gamma p + 3\beta p - 3\beta\beta_1\gamma p - 3\beta - p + 1)$

$$b = -(3\beta^2\beta_1\gamma p + 6\beta p + 3\beta\beta_1\gamma p + 6\beta + 2p - 2)$$

$$c = (2M_c\beta^2 - 2M_c\beta^2 p - 3\beta p + 3\beta + 2p - 1)$$

Thus solving for k and substituting the same in the equation of μ, the value of μ was obtained.

For a given set of material parameters and dimension of the beam section, the moment curvature diagram was generated by substituting an incremental normalized bottom tensile strain β from zero up to failure.

4.4 Load Deflection Response

The load deflection response of a beam was obtained by using the moment curvature response, crack localization rules, and moment area method as follows:

1. For a given cross section and material properties, the normalized tensile strain at the bottom fiber β is incrementally imposed to generate the moment–curvature response using the above given set of equations, and the expressions given in Table 25. For each

value of β in stage 2 and 3, the condition for compressive stress $\lambda < \omega$ or $\lambda > \omega$ is verified in advance of moment–curvature calculation.

2. Since a moment curvature diagram determines the maximum load allowed on a beam section, the discrete moments along the diagram are used to calculate the applied load vector $P = 2M/S$. Where S is a spacing between the support and loading point and $S=L/2$ for three-point bending test.
3. The beam is segmented into finite sections. For a given load step, static equilibrium is used to calculate moment distribution along the beam and moment–curvature relationship along with crack localization rules to identify the curvature.
4. The deflection at mid-span is calculated by numerical moment-area method of discrete curvature between the support and mid-span. This procedure is applied at each load step to until a complete load deflection response is obtained. A simplified procedure for direct calculation of the deflection is presented in the next section.

The load CMOD response for the same can be calculated by obtaining the product of the increasing bottom tensile strain value and the first cracking strain with the plastic length of the beam. Thus, the value of CMOD can be expressed by the following equation.

$$CMOD = \beta_{tbot} \varepsilon_{cr} L_p$$

4.5 Results

A MATLAB code has been developed which helps generate the stress strain plot for changing β values using the above given model if the basic values like the geometry of the section and material parameters like Young's Modulus, First cracking strain, ultimate tensile strain and the normalized residual strength at the first cracking are known. Running this code for generating the responses for the specimen with steel fiber the following combined responses for the static and creep tests are generated.

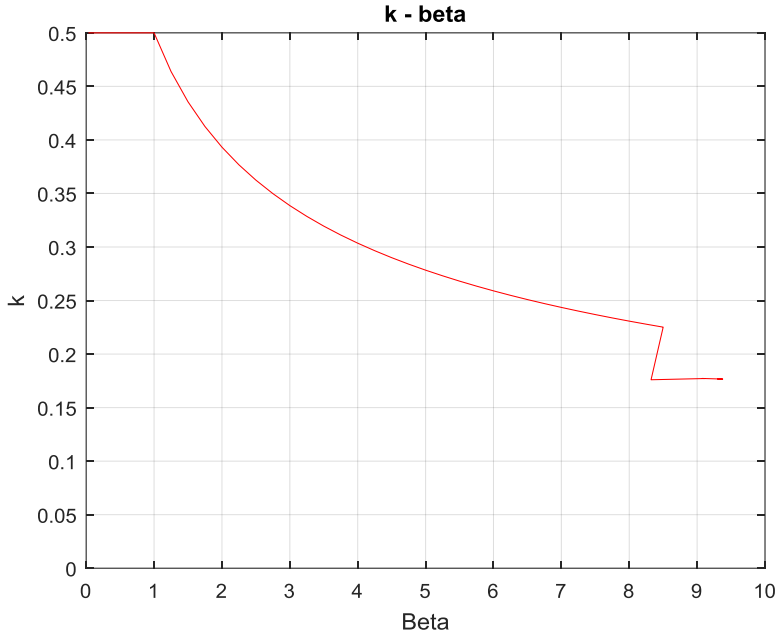

Figure 53:Neutral axis depth ratio versus increasing β value plot for a constant moment and force equilibrium

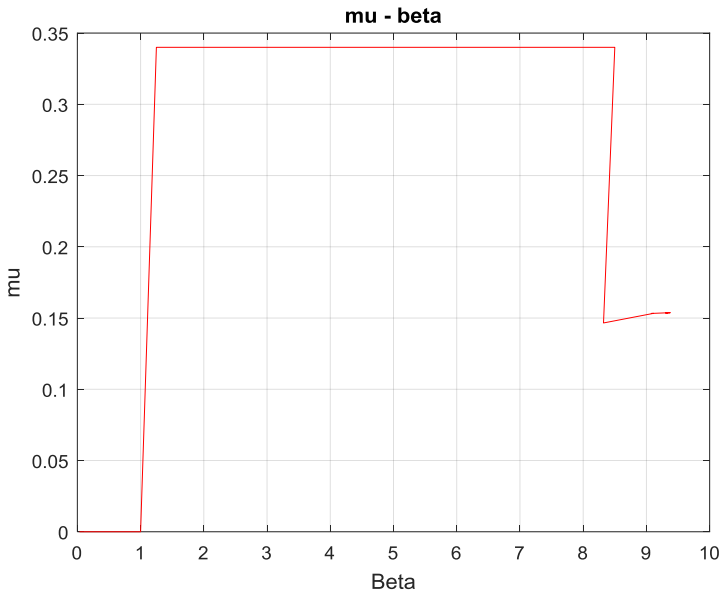

Figure 54: Residual Tensile Strength versus increasing β value plot for a constant moment and force equilibrium

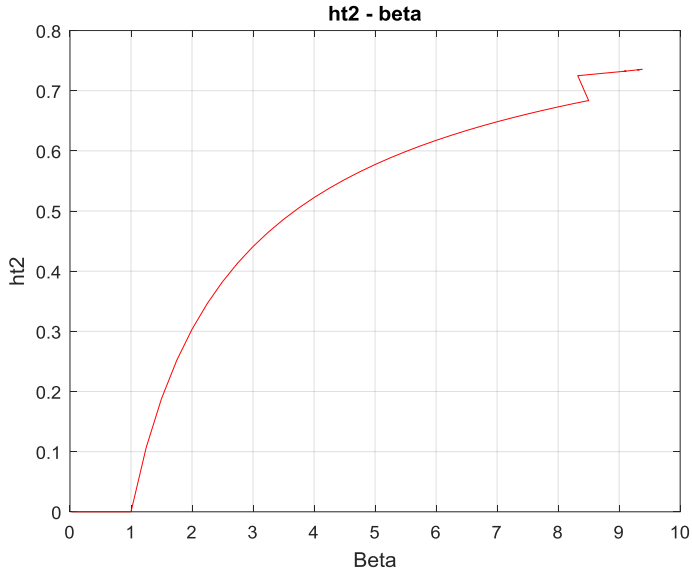

Figure 55: Height of cracked region in stress diagram versus increasing β value plot for a constant moment and force equilibrium

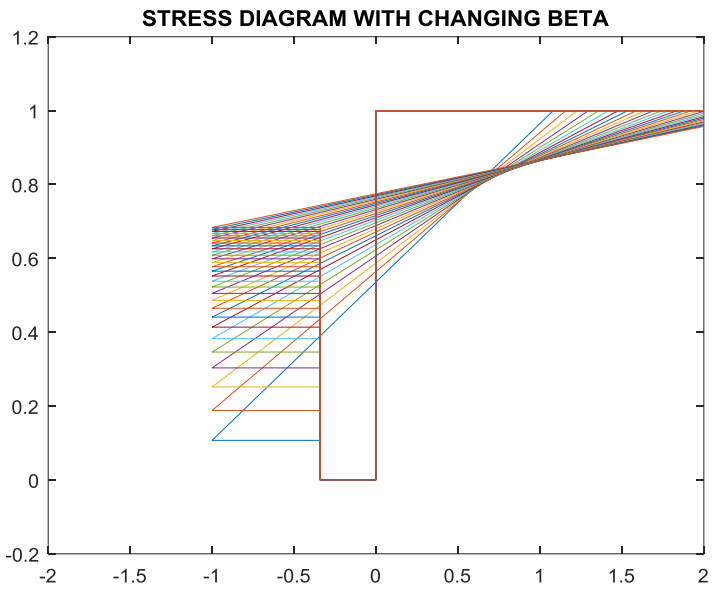

Figure 56: Changing stress plot with an increasing value of β for static loading

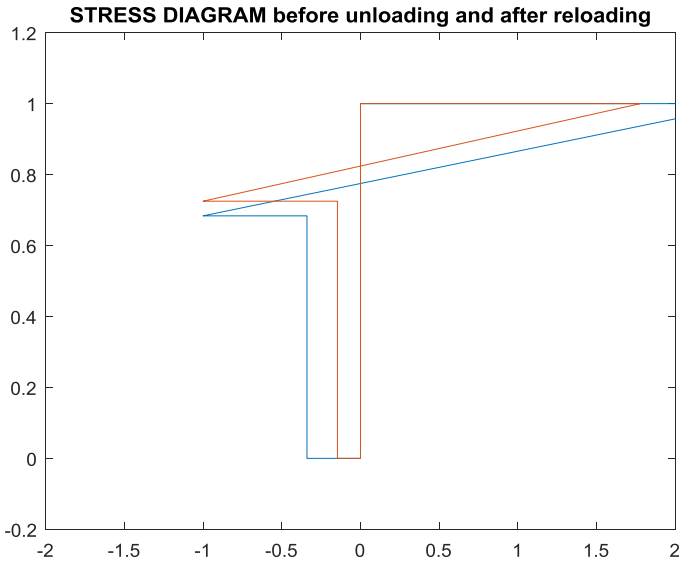

Figure 57: Stress Diagram at FR1 and at the beginning of Creep Loading

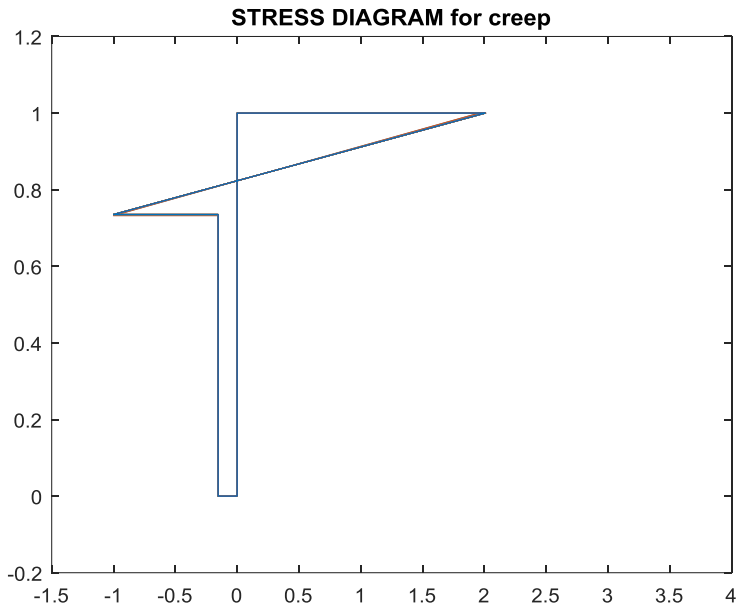

Figure 58: Changing stress plot with an increasing value of β for creep loading

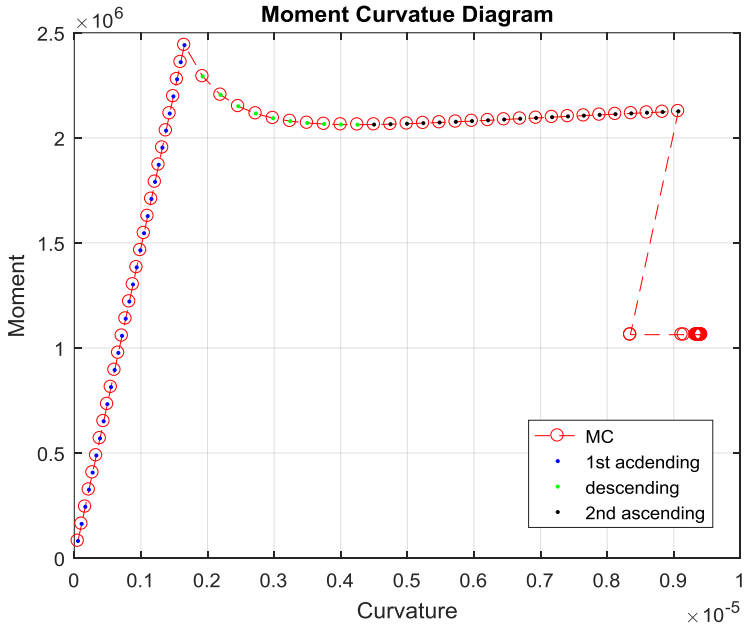

Figure 59: Moment Curvature Response for the Specimen in Static and Creep Loading

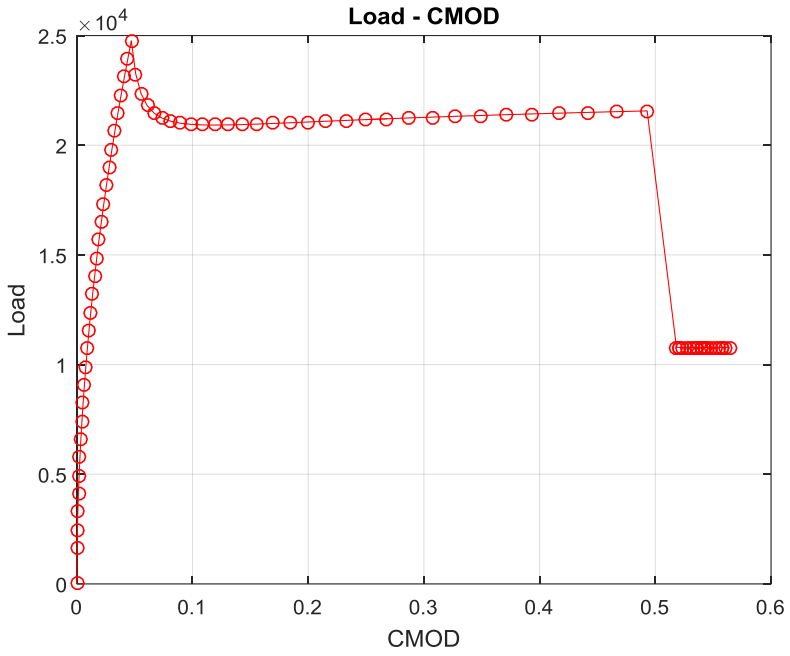

Figure 60:Load versus CMOD response for Static and Creep Loading

Along with generating these plots, the program also generates an output data file which includes the calculated values for normalized compressive strain, neutral axis depth ratio, net forces, curvature, total moment, residual tensile strength and the height of the cracked region in the stress diagram for every incremental value of normalized tensile strain for the static as well as creep loading. A simulation of this model along with the experimental data gives the following response.

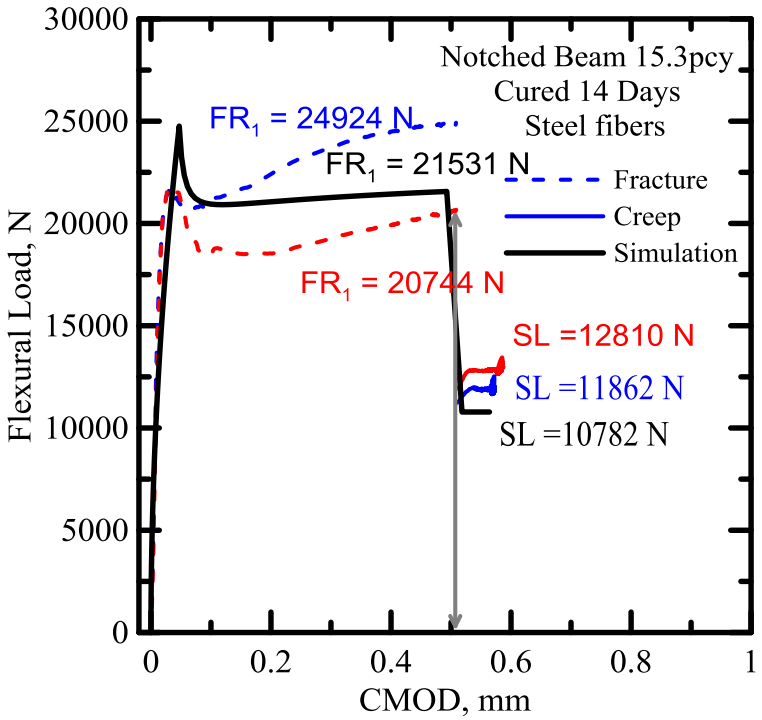

Figure 61: Creep Prediction Model Simulation for specimen with Steel Fibers

The response generated for the specimen reinforced with Polymeric Fiber Type 2 using the same model are given below.

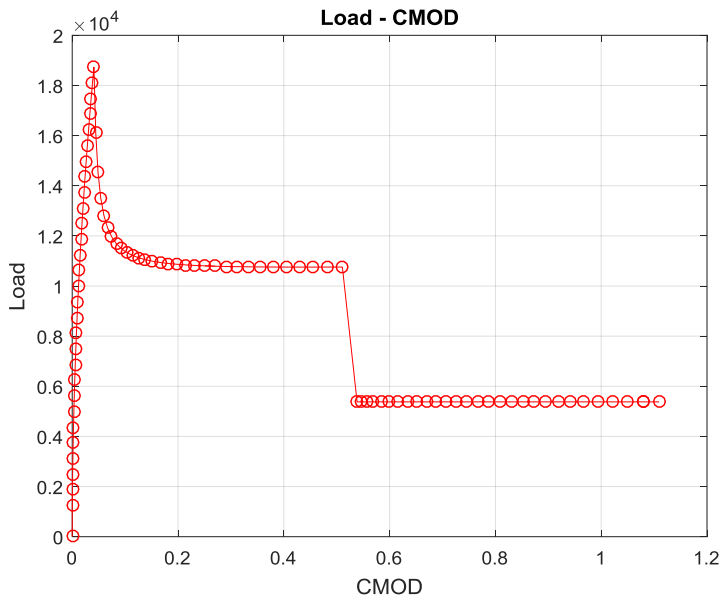

Figure 62: Load versus CMOD response for Specimen with Type 2 Polymeric Fibers

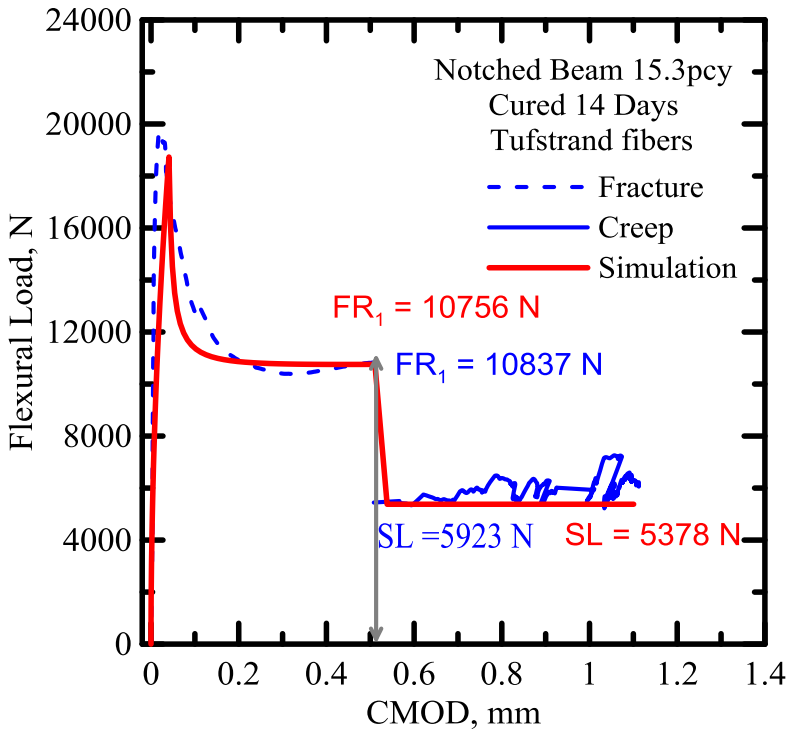

Figure 63: Creep Prediction Model Simulation for specimen with Type 2 Polymeric Fibers

5. Results and Discussions

The discussions for the various experimental analysis and comparative studies carried out have been presented in this section. Various data correlation carried out after a detailed literature review has been given in this section in detail.

5.1 Test Results and Discussions

A combined plot presented by Arango et al [27] incorporated the pre-cracking flexure test result with the unloading stage, the creep loading stage and the final complete flexure test stage. The complete test result diagram is as follows:

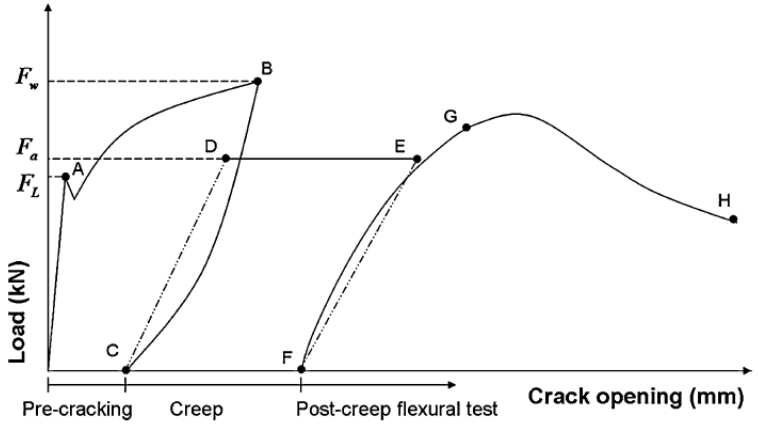

Figure 64: Complete Creep Testing Response [27]

Like the experimental plan, the pre-cracking was carried out on the beam specimens that were supposed to be tested. The test was continued until a desired nominal value 'w_n' of crack width opening was achieved. Various parameters were noted which included the following:

- First Crack Load ($\mathbf{F_L}$)
- Maximum Crack width opening value at the pre-cracking process ($\mathbf{w_p}$).
- Load at w_p ($\mathbf{F_w}$)
- Residual Crack opening width at the pre-cracking process ($\mathbf{w_{pr}}$).

A correlation of the parameters specified in this paper was carried out and the 'Load versus CMOD' and 'CMOD versus Time' graphs were plotted. Two different parameter of creep coefficient were discussed.

The creep tests presented in the paper had two distinct types of specimen and their details are as given below:

Table 26: Specimen Parameters for Creep Testing

Institute	Specimen Name	Fiber	Amount lb/cu.yd	Pre-Crack Opening (inch)	Nominal applied load level (%)
UPV	I-80/35-70-10	Steel Fibers	117.985	0.02	80
ASU	A2_B6_D14_R50	Steel Fibers	66	0.02	50
UPV	II-50/30-40-10	F-Due	67.42	0.02	60

Here the Nominal applied load level was calculated by using the following equation:

$$IFa = \frac{100Fa}{Fw}$$

Where, Fa = Applied Load Level

Fw = Load at the maximum crack opening value at the pre-cracking process.

The following were the CMOD versus Time curves given for the first specimen type.

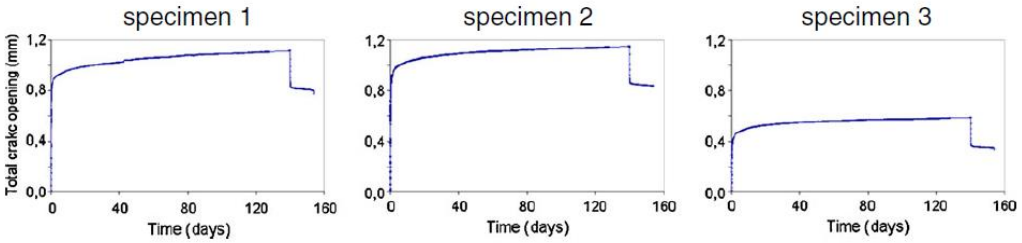

Figure 65: CMOD versus Time curves for I-80/35-70-10 Specimen [27]

A comparative plot of the above-mentioned specimen with the steel fiber specimen of the experiment was generated. It was observed that, using the same type of fibers, the Crack Mouth Opening Displacement values were much higher for higher levels of nominal applied loads.

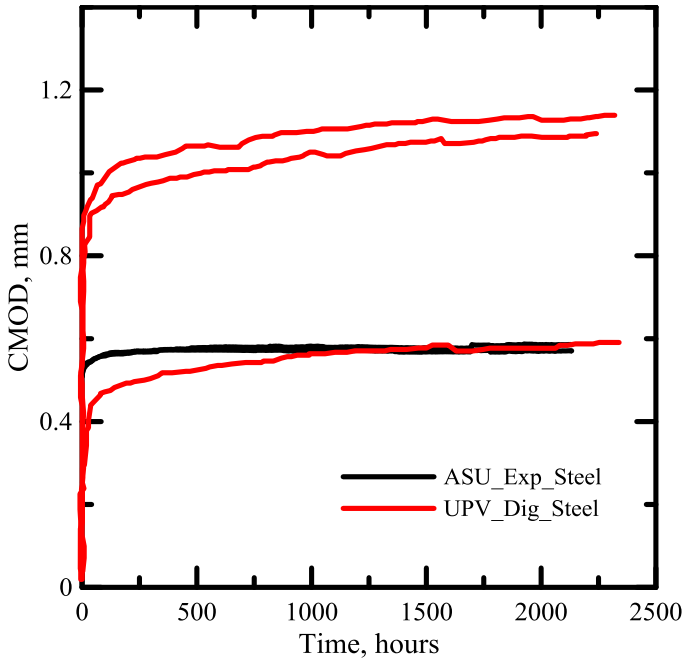

Figure 66: CMOD versus Time Curves for ASU Steel Specimen and UPV Specimen 1

Generating the results for Specimen Type 2 given in the paper, the following results were obtained.

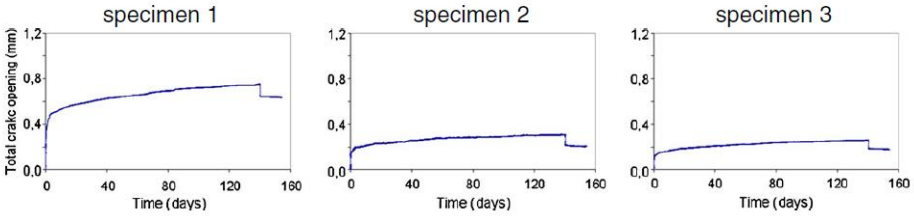

Figure 67: CMOD versus Time curves for Specimen II-50/30-40 [27]

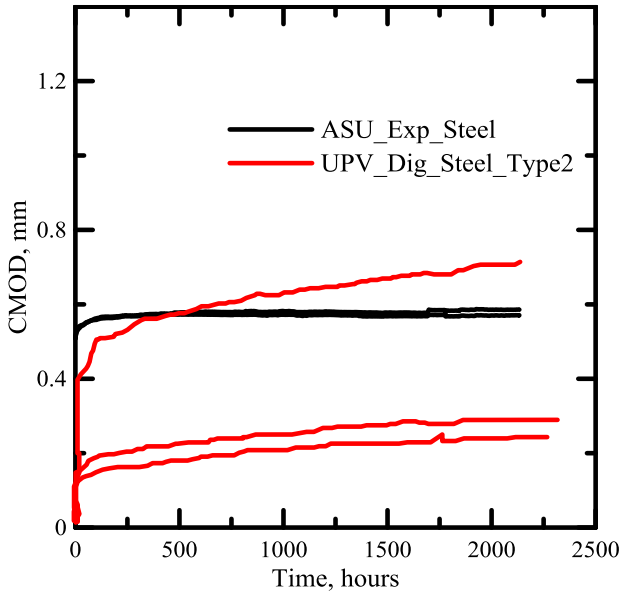

Figure 68: CMOD versus Time Curves for ASU Steel Specimen and UPV Specimen 2

The lower CMOD values for two of the specimens could be explained because of the different fiber type. Burratti et al [28] recommended another approach to carry out the comparative studies of creep experiments. The results of the long-term creep test were analyzed and discussed in two sections which dealt with the following:

- Mid-Span Deflection
- Crack Opening

For the mid span deflection, it was observed that the deflection increased gradually for both the beams over the period of testing of 238 days. Also, it was observed that at the end of the loading phase the value of deflection was similar in both the beams. To make a better comparison of

the behavior of the two beams, a creep coefficient, φ_d, which was related to the mid displacements of the beam was calculated as follows:

$$\phi_d = \frac{\delta(t) - \delta_0}{\delta_0}$$

Where, $\delta(t)$ was the mid span displacement over the general time t, δ_0 was the initial mid displacement and φ_d was the creep coefficient related with the mid span displacement. Another creep coefficient in relation with the 'crack width opening' which was expressed as,

$$\phi_{cr} = \frac{w_t - w_0}{w_0}$$

Where, w(t) was the general crack width at time (t) at the end of the loading phase, w_o was the initial crack width and φ_{cr} was the creep coefficient related with the crack width increment over time. Based on the creep coefficient and the crack width opening, two graphs were presented that show a relative plot of CMOD vs Time and Creep Coefficient vs Time a simulation of the same generated the following plots. The beams were tested for three cracks: A, B and C at varying spans and the crack widths were measured for each of the cracks.

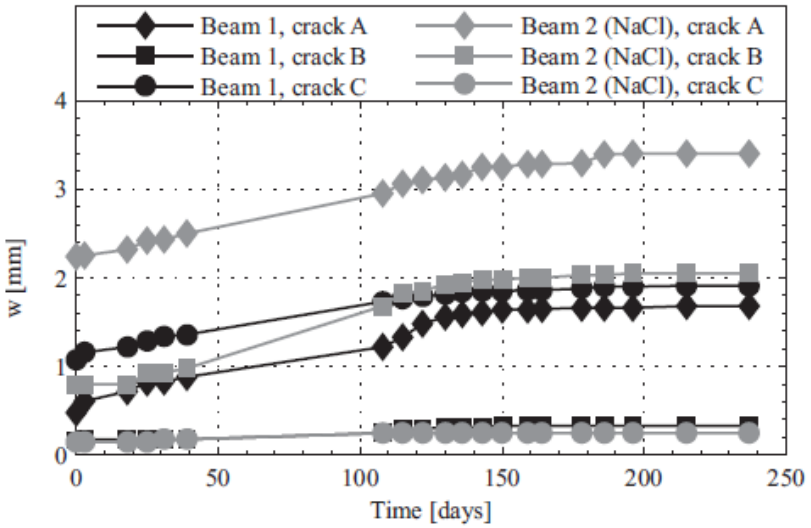

Figure 69: Increase of Crack Width over Time

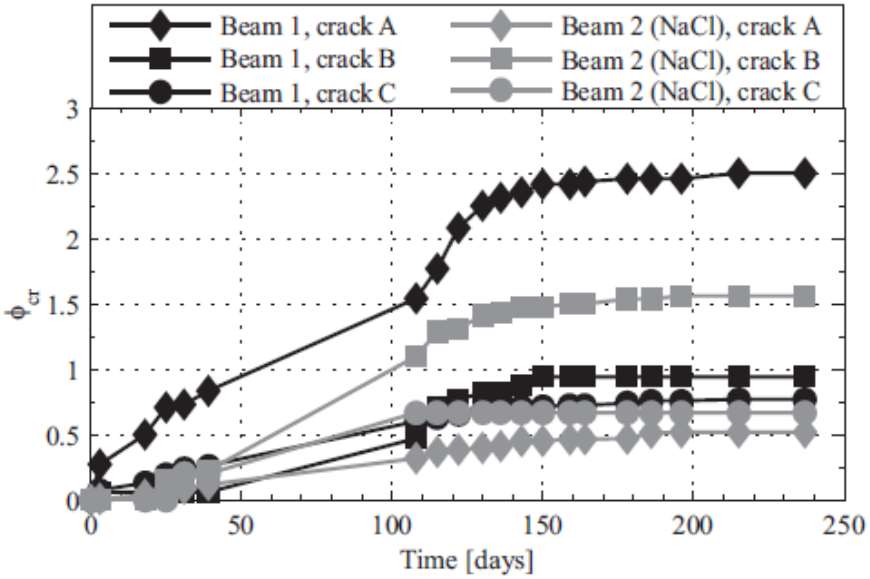

Figure 70: Creep Coefficient Related with Crack Width Opening

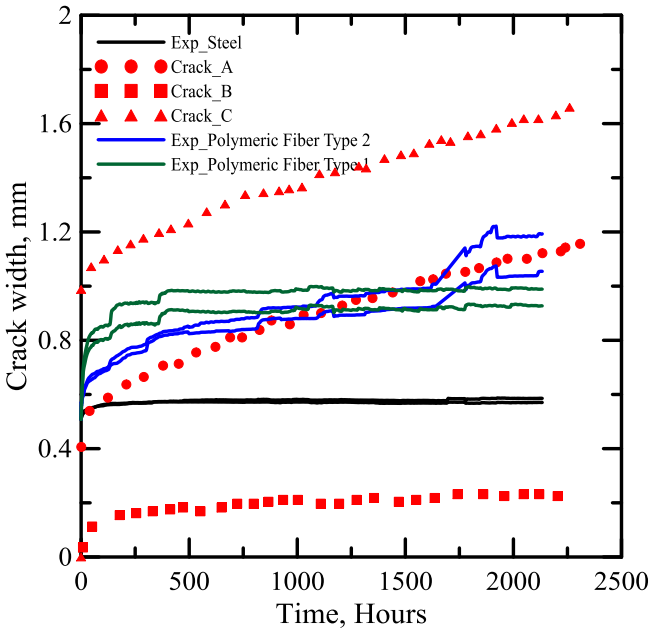

Figure 71: Comparative Crack Width versus Time Plot for Burratti Experimental Data and the Experiemntal Data

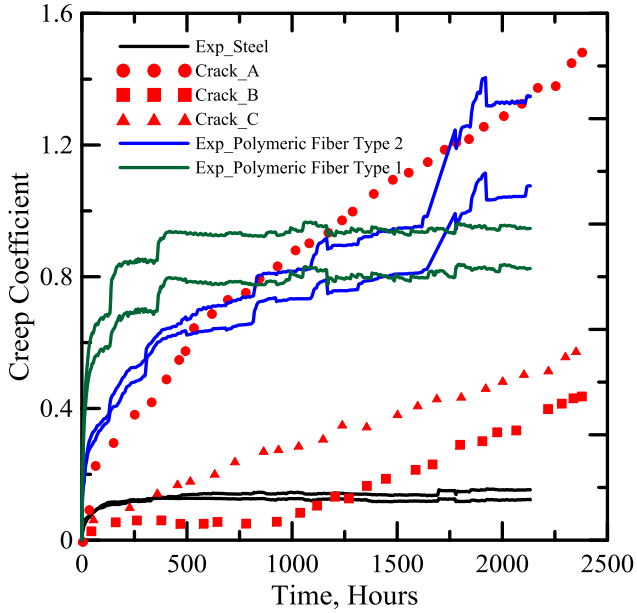

Figure 72: Comparative Creep Coefficient versus Time Plot for Burratti Experimental Data and the Experimental Data

A direct comparison of the test results given by Kurtz et. al. [29] could not be carried out with the experimental results because of two striking differences:

- The difference in test procedures.
- Different data type acquired.

It was observed from the results given that the only beam specimen that sustained the load and did not fail in creep were the ones which were loaded in a range of 30%-38% of service load. Creep failure was observed in the specimen subjected to a loading range of 39%-43% of service load. Rapid failure was obtained for the specimen which were loaded in a range of 50%-88% of service load. Thus an observation was made that the variation in the test procedure and the type of fiber caused an escalated failure.

Creep failure occurred when the stress level was higher than a certain percentage of failure load, however, experimental results disagree with the conclusion.

In contradiction to the analytical result given above, the model proposed by Kohoutkova et al [30] developed on basis of considering the ratios of the basic strength of Fiber Reinforced Concrete to the Plain Concrete. The study suggested that the creep strain of FRC could be predicted as the product of the ratio of the strength of the plain concrete to

the strength of the steel fiber reinforced concrete and the creep strain of the plain concrete.

$$\varepsilon_{f,creep} = \varepsilon_{c,creep} \frac{f_c}{f_f}$$

In order to validate the results obtained by this model an experimental program was adopted. This plan included series of cubes made up of plain concrete and fiber reinforced concrete both being subjected to long term tests. An observation was made that the fluctuations of environmental humidity and temperature did not influence the development of creep strain significantly. The material and shapes of fibers tremendously affected the behavior of the material under creep loads.

The specimen with steel fibers generated better results with lower Crack Mouth Opening Width (CMOD) increasing rate as compared to the polymeric fiber specimen counterparts. Also, an increase in the strain rate was observed with the increase in the volume of synthetic fibers, thus the compressive strength was adopted as the governing factor in the development of prediction model.

5.2 Tertiary Creep Analysis

Under the experimental plan, all the creep responses of the different specimen were stable and stayed within the secondary stage. However, one specimen from the trial batch entered the tertiary stage and eventually

failed. The creep behavior of fiber reinforced concrete in the secondary stage was studied earlier and various functions for predicting the curve and their corresponding parameters were considered.

Tertiary Creep was predicted by generating a response for the experimental data for the failed specimen using the function defined by Stewart et al [31].

To generate the response of damage with respect to time for the experimental data of the failed specimen, the damage parameter was defined as a ratio of CMOD at various time to the final CMOD value at the time of failure, which was given as:

$$damage(d) = \frac{CMOD(t)}{CMOD(\,final)}$$

Thus, the value of Damage ranges up to the maximum value of 1 which notifies failure.

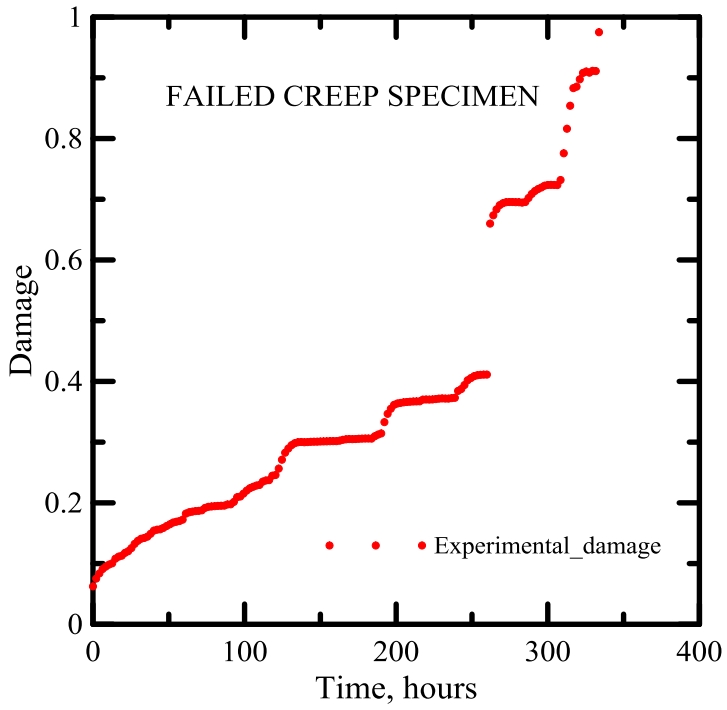

Figure 73: Experimental Damage versus Time plot for Failed Creep Specimen

It was observed that the damage curve started not from zero, but from a value around 0.08. This was explained as the creep tests were carried out on pre-cracked specimen and thus the damage already existed when the creep tests were started. The experimental data was curve fit to understand the nature of the curve and to predict the behavior of the same as an exponential model. This model was a function of the time normalized with respect to the time at which the specimen failed. Thus the equation was given as:

$$damage = ab^{\frac{x}{334.29}}$$

334.29 was the time in hours at which the specimen failed. On curve fitting the equation to the experimental data the following plot was obtained.

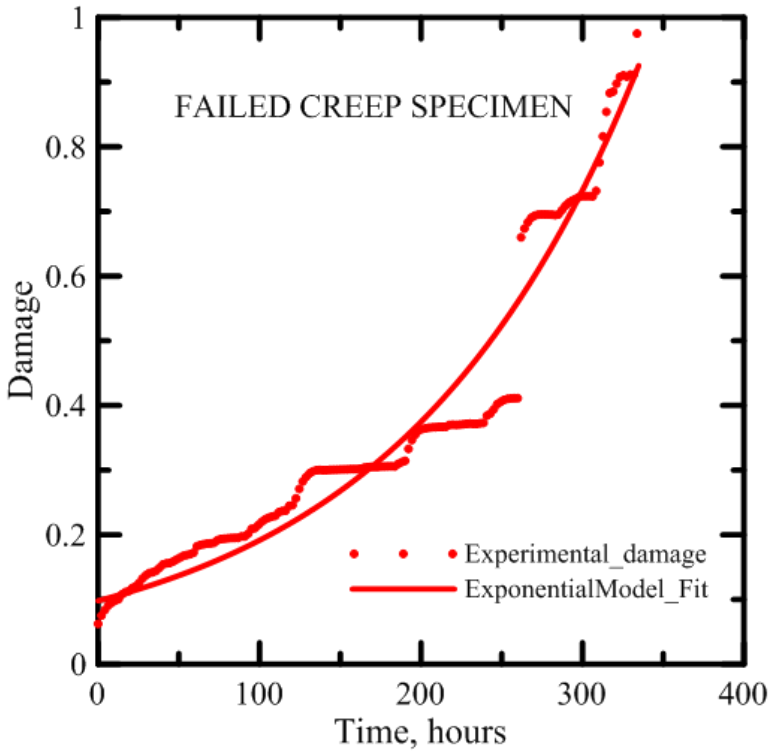

Figure 74: Experimental Damage versus Time plot for Failed Creep Specimen with the Model Curve Fit

Table 27: Curve Fit Values for the Tertiary Creep Exponential Model

Parameter	Value
a	0.09797
b	9.414

In order to verify the model further, it is suggested to carry out more runs of the same on specimen which fail by subjecting them to a higher creep service load.

After gathering experimental creep tests at a constant temperature and different stress levels, the authors have generated a master curve of the normalized experimental data using the equations which are described below. The process has been repeated for a variety of range of temperature sets so as to obtain the temperature dependent function (φ). Given below were the plots obtained after carrying out the entire procedure.

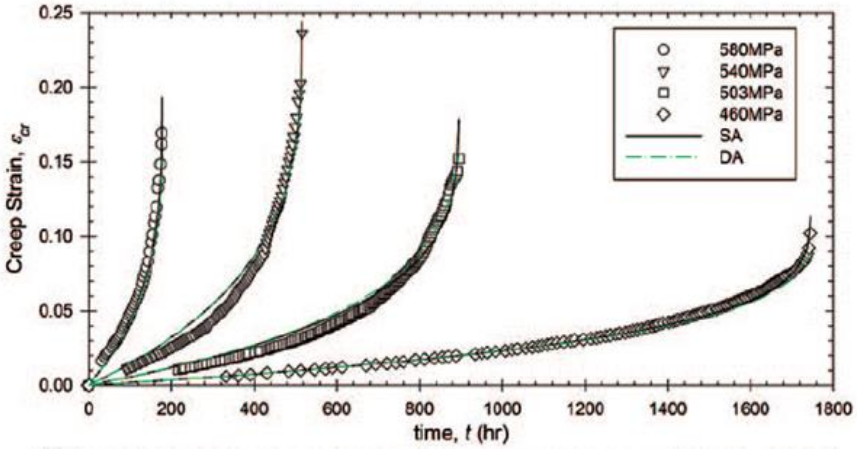

Figure 75: Creep Damage Fit per test by Stewart et al [17]

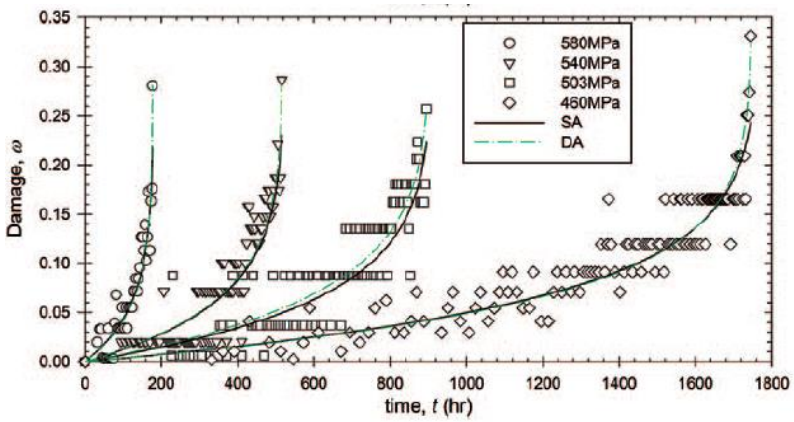

Figure 76: Damage Evolution Fit per Test by Stewart et al [17]

5.2.1 Strain Approach

Here, the damage evolution equation was incorporated in the creep strain rate equation as described in the paper and an indefinite integration was performed which gives the following creep strain formula:

$$\varepsilon_{cr}(t) = \frac{A(\phi+1)[t(\frac{\sigma}{\tau})^n - t_r(\frac{\sigma}{\tau})^n + t_r\sigma^n]}{1+\phi-n}$$

Where, τ is expressed as the following,

$$\tau = (1-\frac{t}{t_r})^{\frac{1}{1+\phi}}$$

Using the available creep strain data, the above given equations and a regression analysis software, the constant φ was determined. However, this function could not be used for simulating the experimental results obtained.

5.2.2 Damage Approach

The damage approach derived data from the creep strain data. Here the damage constant was derived by introducing the M constraint equation into the damage prediction equation giving us the following result:

$$\omega(t) = 1-[\frac{t}{t_r}[(1-\omega_r)^{\phi+1}-1]+1]^{\frac{1}{\phi+1}}$$

Thus, inserting the available damage data, the analytical damage equation and the above given modified damage equation in the regression analysis software, the φ constant was determined.

A simulation of the above given equation was successfully carried out in MATLAB to develop the tertiary creep response for the experimental data.

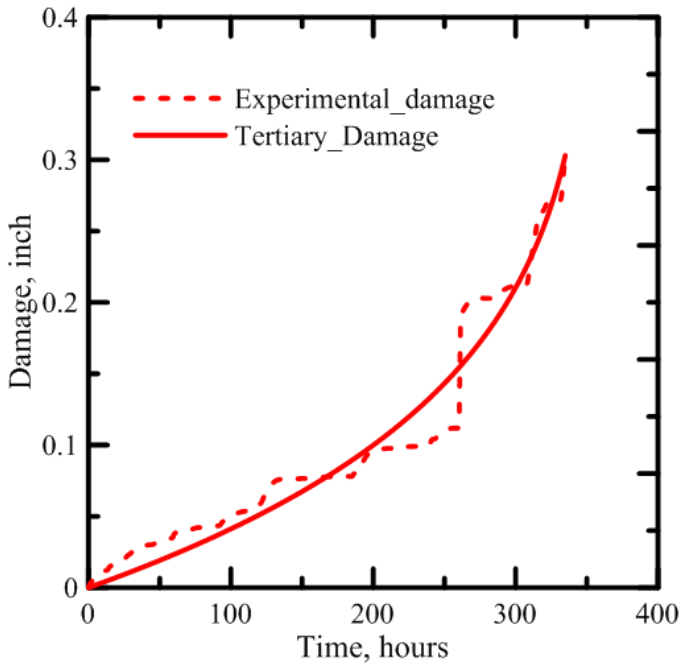

Figure 77: Simulated Experimental Damage Plot for the Failed Experimental Data

The value of the φ constant obtained for the experimental data for the FRC specimen in comparison to the values obtained in the paper are given below.

Table 28: Parameters for the Damage Approach Fit value for the experimental failed specimen

Test	Damage Approach φ
1	18.391
2	15.739
3	14.196
4	15.921
ASU - 1	6.843

5.3 Summary and Future Scope

The purpose of this study was to develop a deeper knowledge about the creep behavior of cracked fiber reinforced concrete under flexure. When concrete cracks in tension, the fibers in the concrete contribute in controlling the crack propagation and increase in the crack width. The main idea of the study was to develop a deeper understanding of the behavior of cracked fiber reinforced concrete under sustained loads and the effects of numerous factors like the type of fibers used, volume fraction of fibers, temperature and humidity conditions etc. on the behavior of cracked fiber reinforced concrete beams.

A detailed literature review was carried out on the existing literature available. Various experimental set ups developed to carry out similar experimental plans were studied. Test results given in the papers were discussed and compared with the experimental data generated for the experimental plan adopted at ASU. It was observed that for similar fiber

types used in fiber reinforced concrete specimen, the response for the crack mouth opening displacement value changed tremendously with an increase in the number of cracks in the specimen. It was also observed that for the same specimen type with the same mix designs and same fiber type, the response for creep can change with a different test set up adopted.

The test set up developed for the creep testing was deduced to be running successfully and with various phases of the experimental plans running, enormous amount of data was collected. Strain hardening kind of behavior was observed for the specimen with steel fibers in it while the specimen with polymeric fiber showed a strain softening kind of behavior. While studying the contribution of three different fiber types for our fiber reinforced concrete specimen, it was observed that the steel fibers helped in controlling the rate of opening of the crack mouth opening displacement much more effectively as compared to the polymeric type of fibers. It was also observed that different polymeric fibers have different responses. The type 1 polymeric fiber is more efficient in the crack growth rate control as compared to the type 2 polymeric fiber.

It was observed that the rate of growth of crack width opening varied with the environmental conditions, however, the final response stayed the same for different temperature conditions. The CMOD growth rate was much higher for the type 1 polymeric fibers under higher temperature of 40ºC as compared to the growth rate for the same specimen at room

temperatures i.e. 21 ºC. Also, it was understood that the higher volume fraction of fibers in the mix design helped the specimen sustain higher loads with a similar crack opening response. Thus, a study was made on all the factors which affected the response of the creep specimen.

Creep compliance values were generated for different specimens tested under the experimental plan. A study of these compliance values was carried out to understand the response of fiber reinforced concrete as a viscoelastic material. Five different viscoelastic models were studied and the model with the best fit compliance was selected for predicting the behavior of fiber reinforced concrete. It was observed that the model with five material parameters fit the experimental compliance the best and the fits got better with increasing number of material parameters in the model.

Creep prediction model was developed to generate a stress strain response of the material and the load CMOD response with respect to increasing bottom tensile strain values. A simulation of this model with the experimental data helped validate the model. Thus, the model could be used further to predict the creep response for a type of fiber reinforced concrete when the basic material parameters are known.

Being a large field of study, the creep testing plan has various future aspects. With the current study involving testing the specimen for 30% and 50% loads of the FR_1, tests can further be carried for higher service loads. Also, the CMOD value at FR_1 can be adopted for different values smaller

or larger to generate the responses and understand the behavior at various cracking levels. The specimens can be subjected to alternating wetting and drying cycles of NaCl solution so as to test the specimen for more exposed environments.

REFERENCES:

[1] Bernard ES, Creep of cracked fiber reinforced shotcrete panels, Shotcrete: More Engineering Developments, Taylor & Francis Group, Page 47-57.

[2] Jenn- Chuan Chern, Chin-Huai Young, Compressive creep and shrinkage of steel fiber reinforced concrete, International Journal of Cement Composites and Lightweight Concrete, Volume 11, Number 4.

[3] Ravindra Gettu, Raul Zerbino, Sujatha Jose, Factors Influencing Creep of Cracked Fiber Reinforced Concrete: What we Think We Know & What We Do Not Know, RILEM 2017, pages 3-12.

[4] Zdenek Bazant, Mija M. Hubler, Qiang Yu, Damage of Prestressed Concrete Structuresdue to Creep and Shrinkage of Concrete, Handbook of Damage Mechanics, Page 515-563.

[5] Rutger Brijdaghs, Marco di Prisco, Lucie Vandewalle, Creep Deformations of Structural Polymeric Macrofibers, RILEM Bookseries 14, Page 56-61

[6] Tomoya Nishiwaki, Sukmin Kwon, Hiroto Otaki, Go Igarashi, Faiz U.A. Shaikh, Alessandro P. Fantilli, Experimental Study on Time-Dependent Behaviour of Cracked UHP-FRCC Under Sustained Loads. RILEM Bookseries 14, Page 101-110.

[7] Nicola Burratti, Claudio Mazzotti, Creep Testing Methodologies and Result Interpretation, RILEM Bookseries 14, Page 13-24.

[8] S.E.Arango, P.Serna, Jose Rocio Marti-Valencia, Emilio Garcia Taengua, A Test Method to characterize Flexural Creep Behaviour of Pre-Cracked FRC Specimen, Experimental Mechanics, October 2012.

[9] N. Burratti, C. Mazzotti, M. Savoia, Long Term Behavior of Cracked SFRC Beams Exposed to Aggressive Environment, Fracture Mechanics of Concrete and Concrete Structures, May 2010.

[10] S. Van Bergen, S. Pouillon, G. Vitt, Experiences from 14 Years of Creep Testing of Steel and Polymer Fiber Reinforced Concrete, RILEM Bookseries 14, Pages 41-52

[11] MacKay, J. Trottier, Post crack creep behavior of steel and synthetic FRC under flexural loading, Shotcrete: More Engineering Developments, Page 47-57.

[12] S. Kurtz, P. Balaguru, Post Crack Creep of Polymeric Fiber Reinforced Concrete in Flexure, Cement and Concrete Research, 2000, Page 183-190.

[13] Alena Kohoutkova, Jan Vodicka, and Vladimir Kristek, Creep and Shrinkage of Fiber-Reinforced Concrete and a Guide for Modelling, ASCE Concreep 10, Page 707-713.

[14] S.E.Arango, P.Serna, Jose Rocio Marti-Valencia, Emilio Garcia Taengua, A Test Method to characterize Flexural Creep Behaviour of Pre-Cracked FRC Specimen, Experimental Mechanics, October 2012.

[15] S. Kurtz, P. Balaguru, Post Crack Creep of Polymeric Fiber Reinforced Concrete in Flexure, Cement and Concrete Research, 2000, Page 183-190.

[16] ASTM C 1399-98, Test Method for obtaining average residual strength of fiber reinforced concrete, Annual Book of ASTM Standards, Vol. 04.02., 1998.

[17] Calvin M. Stewart, Ali P. Gordon, Strain & Damage Based Analytical Methods to Determine the Kachanav-Rabotov Tertiary Creep-Damage Constants, International Journal of Damage Mechanics, November 2012

[18] EN, B. (2007). 14651. Test method for metallic fiber concrete measuring the flexural tensile strength (limit of proportionality (LOP), residual). UK: BSI, 1-20.

[19] Bernard, E.S. Durability of Fiber Reinforced Shotcrete, "Shotcrete: more Engineering Developments, Bernard, Ed., Taylor and Francis, London, pp. 59-64, 2004.

[20] ASTM C1550-05 Standard Test Method for Flexural Toughness of Fiber Reinforced Concrete (Using Centrally Loaded Round Panel), American Society of Testing and Materials, Philadelphia, PA, 2005.

[21] P. Pujadas, Ana Blanco, Sergio H.P. Cavalaro, Albert de la Fuente, A. Aguado, Flexural Post Cracking Creep Behaviour of Macro-synthetic and Steel Fiber Reinforced Concrete, RILEM Bookseries 14, Page 77-87.

[22] Reinhardt, Hans-Wolf, Deformation Behavior of Self-Compacting Concrete under Tensile Loading, Materials and Structures, 2007, Page 965-977.

[23] Rossi, Pierre; Tailhan , Jean-Louis; Boulay, Claude; Maou, Fabrice Le; Martin, Eric; Compressive, Tensile and Bending Basic Creep behaviours related to the same concrete, Structural Concrete 14 No. 2, 2013, Page 124-130.

[24] Rossi, Pierre; Tailhan , Jean-Louis; Boulay, Claude; Maou, Fabrice Le; Martin, Eric; Compressive, Tensile and Bending Basic Creep behaviours related to the same concrete, Structural Concrete 14 No. 2, 2013, Page 124-130.

[25] Zhu, Chen, & Yang, Prediction of Viscoelastic Behaviour in Asphalt Concrete Using the Fast Multiple Boundary Element Method, Journal of Materials in Civil Engineering, ASCE, page 328-336, March 2013.

[26] Chote Soranakom, Barzin Mobasher, Correlation of tensile and flexural responses of strain softening and strain harening cement composites, Cement & Concrete Composites, January 2008.

[27] S.E.Arango, P.Serna, Jose Rocio Marti-Valencia, Emilio Garcia Taengua, A Test Method to characterize Flexural Creep Behaviour of Pre-Cracked FRC Specimen, Experimental Mechanics, October 2012.

[28] N. Burratti, C. Mazzotti, M. Savoia, Long Term Behavior of Cracked SFRC Beams Exposed to Aggressive Environment, Fracture Mechanics of Concrete and Concrete Structures, May 2010.

[29] S. Kurtz, P. Balaguru, Post Crack Creep of Polymeric Fiber Reinforced Concrete in Flexure, Cement and Concrete Research, 2000, Page 183-190.

[30] Alena Kohoutkova, Jan Vodicka, and Vladimir Kristek, Creep and Shrinkage of Fiber-Reinforced Concrete and a Guide for Modelling, ASCE Concreep 10, Page 707-713.

[31] Calvin M. Stewart, Ali P. Gordon, Strain & Damage Based Analytical Methods to Determine the Kachanav-Rabotov Tertiary Creep-Damage Constants, International Journal of Damage Mechanics, November 2012